Search for continuous gravitational wave emission from the Milky Way center in O3 LIGO-Virgo data

R. Abbott *et al.*[*]
(LIGO Scientific Collaboration, Virgo Collaboration, and KAGRA Collaboration)

(Received 9 April 2022; accepted 29 June 2022; published 9 August 2022)

We present a directed search for continuous gravitational wave (CW) signals emitted by spinning neutron stars located in the inner parsecs of the Galactic Center (GC). Compelling evidence for the presence of a numerous population of neutron stars has been reported in the literature, turning this region into a very interesting place to look for CWs. In this search, data from the full O3 LIGO-Virgo run in the detector frequency band $[10, 2000]$ Hz have been used. No significant detection was found and 95% confidence level upper limits on the signal strain amplitude were computed, over the full search band, with the deepest limit of about 7.6×10^{-26} at $\simeq 142$ Hz. These results are significantly more constraining than those reported in previous searches. We use these limits to put constraints on the fiducial neutron star ellipticity and r-mode amplitude. These limits can be also translated into constraints in the black hole mass–boson mass plane for a hypothetical population of boson clouds around spinning black holes located in the GC.

DOI: 10.1103/PhysRevD.106.042003

I. INTRODUCTION

The Milky Way's center is one of the most interesting sky regions and is well suited to investigations with multiple messengers, ranging from electromagnetic radiation and cosmic rays to gravitational waves (GWs). A significant population of up to hundreds or even thousands of neutron stars is expected to exist in this region, based on the observation of high-mass progenitor stars and of several supernova remnants [1,2]. Moreover, an extended gamma-ray emission from the central region of the Galaxy has been detected by the *Fermi* Large Area Telescope [3,4] and H. E. S. S. [5]. The true nature of this emission is still under debate, with two main competing explanations: annihilation of dark matter in the form of weakly interacting massive particles, with masses of the order of a few tens of GeV [6–10], or an unresolved population of millisecond pulsars [11–17]. This diffuse emission may also actually be due to a combined contribution from both a population of millisecond pulsars and heavy dark matter [18].

The possibility that the Galactic Center (GC) region hosts a large population of neutron stars calls for the search for continuous gravitational waves (CWs) that neutron stars would emit if their shape deviated from axial symmetry. Although previous searches have not reported any detection (see the reviews [19–22] and references therein plus the last results in [23–29]), improvements in detectors and data analysis pipelines [30] can increase the search sensitivity to a level at which detections can take place.

In this work we present the results of a search, using the latest data from the third observing run (O3) of the Advanced Virgo [31] and Advanced LIGO [32] detectors, for CWs emitted by nonaxisymmetric rotating neutron stars located in the GC region. This work, based on the band-sampled-data (BSD) directed search pipeline [33,34], improves over a previous search in O2 data [34].

O3 data have been already used to make a lower sensitivity search for stochastic GW emission from the same region [35].

Potentially detectable CW emission is expected from Galactic, fast-spinning neutron stars with a certain degree of asymmetry in their mass distribution [22,36]. As the star spins, it releases energy in the form of GWs, which are almost monochromatic and characterized by an emitted frequency proportional to the star's spin frequency. The frequency received at a detector evolves in time due to two main contributions. One comes from the intrinsic frequency decrease (spin down) caused by energy loss of the star. The other is due to the Doppler modulation of the received signal, caused by the motion of the detector with respect to the source. Other smaller effects are also considered, namely the Einstein and the Shapiro delays.

The asymmetry in the neutron star's shape can be due to different reasons. They include the presence of a residual crustal deformation (e.g., after a fast cooling of the neutron star crust causing its breaking), the presence of a strong internal magnetic field not aligned with the star's rotation axis, or the presence of magnetic or thermal "mountains." The maximum ellipticity (i.e., degree of deformation) a neutron star can sustain depends on both its equation of

[*]Full author list given at the end of the article.

state (EOS) and the breaking strain of the crust [37]. On the other hand, the typical degree of asymmetry is difficult to estimate. The detection of a CW signal would help to shed light on the internal structure of neutron stars, hence on the EOS, given the relation of the GW amplitude to the star's moment of inertia and the star's ellipticity. GWs are then unique probes of the fundamental interactions happening inside a neutron star, making them ideal laboratories to test fundamental physics and high-energy astrophysics in the strong-gravity regime [38]. A different emission channel for CW radiation is given by the Rossby (r-)modes oscillations in rotating stars [39–41].

The emission of CWs is also expected from other sources, not involving neutron stars. For instance, it has been predicted [42–50] that if ultralight boson particles (a dark matter candidate) exist in nature, they may spontaneously form macroscopic "clouds" around spinning black holes through a *superradiance* process (provided that the black hole initial spin is high enough). Once formed such clouds dissipate through the emission of a CW signal, with a frequency mainly depending on the boson mass. In this work we also use the CW search results to constrain a possible boson cloud population in the GC.

The paper is organized as follows. In Sec. II, the data used for the analysis are described. Section III is devoted to discussing the explored parameter space and the main search method. Postprocessing is presented in Sec. IV, including all the vetoes used to discard instrumental artifacts. In Sec. V, we present the search results and their astrophysical implications, for spinning neutron stars and for boson clouds around spinning black holes. In Sec. VI, conclusions are drawn. Some details on the upper limits computation are given in the Appendix.

II. THE DATA

For this search we have used the full O3 data of the two Advanced LIGO detectors in Hanford (H) and Livingston (L) in the United States [32] and of Advanced Virgo (V) in Cascina, Italy [31]. The O3 observing run started on April 1, 2019 at 15:00 UTC and ended on March 27, 2020 at 17:00 UTC. During data taking there was a one-month break, from October 1, 2019 to November 1, 2019. The duty factors for O3 were 76%, 71%, and 76% for L, H, and V, respectively. The sensitivities of the three detectors are comparable at lower frequencies, while Virgo sensitivity above ∼100 Hz is smaller than the other two LIGO detectors. The last version of the high-latency calibrated data (C01 frames) [51] has been used for H and L, while for Virgo the "online" calibration version has been used. Moreover, only science segments, i.e., time intervals when the detector is operating in a nominal state and the noise level is considered as acceptable, have been selected. The maximum calibration amplitude uncertainties for LIGO are 7% during the first half of O3 (O3a) [51] and 11% during the second half of O3 (O3b) [52]. For Virgo the calibration uncertainty is 5% in amplitude for the full frequency band except for regions around 50 Hz where larger uncertainties appear [53]. A gating procedure has been applied to LIGO data as described in [54] to remove larger transient artifacts. Furthermore, for all the detectors, short-duration noise transients have been removed during the construction of the short Fourier transform database (SFDB) [55]. The search is based on the BSD framework [33], which works with time series sampled at 10 Hz and spanning a 10-Hz frequency band, computed from the SFDB. Indeed in the BSD framework, the parameter space investigated, as well as the choice of the grid steps and the coherence time used, change every 10 Hz. Given the limited computational power available, the parameter space investigated has been chosen satisfying some constraints described in Sec. III A. Spectral noise artifacts, known as lines, are also present in detector data. Lists of narrow lines with identified instrumental origin are given in [56,57]. These lists will be used in the postprocessing stage, to veto candidates near instrumental lines (see Sec. IV A).

III. THE SEARCH

The search is conducted with a semicoherent method [34] in which the data are divided into segments of given duration T_{coh}. These segments are properly processed, as will be clarified in Sec. III B, and then incoherently combined, i.e., not taking into account the signal phase. In this way we can explore a large parameter space at a fixed computing cost, with only a relatively small sensitivity loss with respect to an optimal, fully coherent procedure when applied in an all-sky search (see, e.g., Sec. XII D in [58]). In this search we do not explicitly search for CW signals from neutron stars with a binary companion. However, as discussed in [59], the results presented in this work are valid to some extent also for accreting binaries.

A. Parameter space

We look for persistent signals from sources emitting in the detector frequency band $[10, 2000]$ Hz and located in the GC, with a maximum spin-down range of $[-1.8 \times 10^{-8}, 10^{-10}]$ Hz/s. The actual minimum value of the spin down is a function of the search frequency, as we will clarify below; see also Fig. 1.

The parameter-space volume is discretized in several cells. The key quantity governing the discretization is the segment duration T_{coh}. Its value is chosen as a function of the frequency to keep the signal frequency at the detector, which varies due to the spin down and Doppler effect, within one frequency bin, given by $\delta f = 1/T_{\mathrm{coh}}$. In each 10-Hz band, the smallest T_{coh} is adopted for the whole band. The corresponding number of frequency bins is $10\ \mathrm{Hz} \times \mathrm{T_{coh}}$. The spin-down bin size is given by

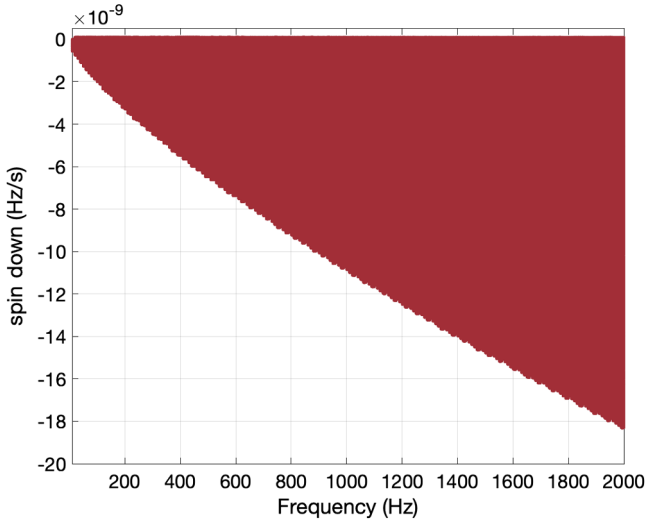

FIG. 1. Parameter space investigated in this search (see Sec. III A). The sky position is that of Sgr A*, while frequency and spin down span the ranges given on the axes.

$$\delta\dot{f} = \frac{1}{2T_{\mathrm{obs}}T_{\mathrm{coh}}}, \tag{1}$$

where T_{obs} is the total observing time. This is computed by imposing that the associated frequency variation over the observation time T_{obs} is at most half a bin. This choice is more conservative than the one in [58], where the maximum frequency variation is of one bin.

The bin width for the second order spin down is

$$\delta\ddot{f} = \frac{1}{4T_{\mathrm{obs}}^2 T_{\mathrm{coh}}}. \tag{2}$$

To minimize the computational load of the analysis, we consider a single value for the second order spin down, i.e., $N_{\ddot{f}} = 1$. The number of second order spin-down bins depends on the parameter space investigated and the search setup, $N_{\ddot{f}} = 2N_f(T_{\mathrm{obs}}|\dot{f}|/f)^2$, which always satisfies the condition $N_{\ddot{f}} \leq 1$ for this search. For balancing the computational cost among the available resources, and taking into account the available CPU memory, a different range of spin-down values is computed for every 10-Hz band, resulting in a smaller minimum value at low frequencies. The number of spin-down/spin-up bins $N_{\dot{f}}$ is then given by the $\dot{f}$ range covered in each 10-Hz band divided by the corresponding $\delta\dot{f}$. The minimum spin down goes from -5.6×10^{-10} Hz/s in the band 10–20 Hz to -1.8×10^{-8} Hz/s in the band 1990–2000 Hz band. This choice corresponds to a value of a characteristic spin-down age[1] $\tau = f/|\dot{f}|$ that goes from ≃570 yr at 10 Hz to ≃3520 yr at 2000 Hz. The small range of positive $\dot{f}$, from 0 to 10^{-10} Hz/s in the full frequency band, allows us to take into account a possible spin up, as expected for the signal emitted by boson clouds around spinning black holes. The frequency/spin-down ranges covered by the search are shown in Fig. 1. The estimated computing cost per detector is ∼500 core hours for jobs running on a Intel ES-2640V4 CPU.

Concerning the sky, only one bin centered at the position of Sgr A* [60] with right ascension $\alpha_{\mathrm{GC}} = 17\ \mathrm{h}\,45\ \mathrm{m}\,40.04\ \mathrm{s}$ and declination $\delta_{\mathrm{GC}} = -29°00'\ 28.1''$ is taken into account. With the values of T_{coh} we are using, one sky bin covers 30–300 pc, depending on the frequency [34], which is wide enough to include the most interesting region around the GC.

B. Method

For this work we use the hierarchical semicoherent BSD directed search pipeline [34] based on the FrequencyHough (FH) transform [58,61], recently used in the search for CW signals from supernova remnants in our Galaxy [27] and previously used for a GC search in Advanced LIGO O2 data [34].

In this search, we first partially correct the time series, separately for each detector, removing the Doppler modulation in each 1-Hz frequency subband, using its central frequency as a reference (see [34] for more details). This is achieved by a "heterodyne" correction, i.e., multiplying the time series by a complex exponential factor $e^{i\Delta\phi}$, where $\Delta\phi$ is the signal phase variation associated with the Doppler effect and referring to the central frequency of each 1-Hz band within a 10-Hz band.

The second step of the search consists of the selection of the most significant peaks (collectively called "peak map") in the time-frequency plane. In order to do this, first *equalized* spectra [55] are evaluated. They are obtained as the ratio among the periodogram, given by the square modulus of the Fourier transform of each data segment with duration T_{coh} and an average spectrum estimation. On the ratio, all the local maxima above a given threshold are selected. Each of these "peaks" is defined by a frequency and by the initial time of the corresponding data segment of length T_{coh}. Each peak map covers 10 Hz in frequency and one month in time.

The peak map is then passed to the third step of the analysis, which consists of the FH transform. The FH transform maps each time-frequency peak to the intrinsic source frequency and spin-down $(f_0, \dot{f}_0)$ plane at a given reference time t_0. As described in [58] each time-frequency peak in the peak map becomes a line in the FH plane. Hence, each pixel of the FH map has an associated number count n, corresponding to the number of lines intersecting in that point. The resolution of a single FH map is related to the coherence time T_{coh} used for the construction of the peak maps. The resolutions in frequency and spin down are given by

[1]This is a rough measure of the star's age, which assumes the initial spin frequency is much higher than the current one.

$$\delta f_{\mathrm{FH}} = \frac{1}{T_{\mathrm{coh}} K_f}, \tag{3}$$

$$\delta \dot{f}_{\mathrm{FH}} = \frac{1}{T_{\mathrm{coh}} T_{\mathrm{obs}} K_{\dot{f}}}. \tag{4}$$

The parameters K_f and $K_{\dot{f}}$ are the over-resolution factors as described in [58], here chosen as $K_f = 10$ and $K_{\dot{f}} = 2$. Given the low computing cost of this search, we use $K_{\dot{f}} = 2$, while in the all-sky search setup of [58], there is no over-resolution factor used for the spin-down grid. With this choice the FH spin-down bin is equivalent to the one defined in Eq. (1).

For each 10-Hz band, this process is repeated for each month of data and the single FH maps are summed up into a final map. On this we select outliers, i.e., pairs $(f_0, \dot{f}_0)$ with high significance. More specifically, for each 0.01-Hz subband and for each spin-down subband,[2] we take the two strongest outliers. In this way a maximum of ∼2000 outliers are selected in each map and for each spin-down subband. The total number of outliers in the search is 3410398 for L, 3409029 for H, and 3408485 for V. The strength of an outlier is expressed through the critical ratio (CR) defined as

$$\rho_{\mathrm{CR}}(n) = \frac{n - \mu_n}{\sigma_n}, \tag{5}$$

where μ_n and σ_n are the mean and the standard deviation of the FH number count n, respectively. The CR of an outlier corresponds to a significance, expressed, e.g., in terms of p-values, compared to the expected CR distribution under the hypothesis that the data do not contain any signal and assuming a Gaussian noise distribution.

Coincidences among pairs and triplets of outliers found in the data of the three detectors are computed. Coincidences among two outliers are defined on the base of a dimensionless distance defined as [58]

$$d = \sqrt{\left(\frac{\Delta f}{\delta f_{\mathrm{FH}}}\right)^2 + \left(\frac{\Delta \dot{f}}{\delta \dot{f}_{\mathrm{FH}}}\right)^2}, \tag{6}$$

where Δf and $\Delta \dot{f}$ are the differences between the outlier parameters. All the pairs of outliers from two different detectors [i.e., Hanford-Livingston (HL), Hanford-Virgo (HV), and Livingston-Virgo (LV)] with a distance smaller than $d_{\mathrm{thr}} = 4$ pass to the postprocessing stage [27,34]. Moreover, mean parameters of coincident HL outliers are used to compute the distance from V outliers, using the same criterion as before, selecting in this way triple coincidences, which are subject to a similar postprocessing.

A total of 2142 triple HLV coincidences have been found, mostly from candidates with spin up. Double coincidences are 37570 for HL, 36988 for HV, and 37455 for LV. Given the lower sensitivity of the Virgo detector compared to Hanford and Livingston at higher frequencies, we only keep those double-coincident candidates below 100 Hz, reducing the number of HV and LV coincidences to 381 and 458, respectively. This choice is justified by the fact that a real signal showing a significant result in the Virgo detector above 100 Hz should necessarily be evident also in the HL coincidence set.

To screen out insignificant outliers, we select only the double coincidences with a $\rho_{\mathrm{CR}}(n) > \rho_{\mathrm{CR,thr}}$. The threshold is chosen considering the probability of picking, on average over each 10-Hz band, 500 false single-detector candidates over the total number of spin-down bins, under the assumption of Gaussian noise. The threshold used is $\rho_{\mathrm{CR,thr}} \simeq 4.78$ and it is the same for each dataset. This threshold is also very close to the mean ρ_{CR} plus 1 standard deviation of the CR distribution across the single-detector candidates excluding those due to known instrumental lines. This step is described in Sec. IV A. From a computational point of view, using a higher threshold would have certainly reduced the number of potential candidates for further investigation. However, this would also increase the false-dismissal probability. For the triple HLV coincidence set we focused on those candidates above $\rho_{\mathrm{CR,thr}}$, including those with a frequency below 100 Hz, independent of their CR.

IV. POSTPROCESSING

Before passing to the follow-up stage, the outliers selected during the coincidence step undergo a series of vetoes. The set of vetoes is applied on all the coincident outliers discarding those having at least one of the following features: they overlap in frequency with known spectral lines (in at least one of the detectors); they are not consistent with the expected significance in each detector (higher significance is expected to arise from the most sensitive detector). These vetoes are described in more detail in the following sections.

A. Lines veto and consistency check

Due to the presence of instrumental artifacts [62] (typically spectral lines [63]), which affect the data quality, outliers lying in a frequency band polluted by a known noise line [56,57] are vetoed. A candidate is then vetoed if during the run its frequency intersects with the frequency region affected by the spectral line. This veto step is applied before coincidences. At this stage, ∼8.0% of the outliers are removed from the H dataset, while ∼4.6% and ∼4.9% are removed from L and V, respectively.

[2]To minimize the computational load of each analysis job, the full spin-down range has been divided into a few subbands, going from 9 for all the bands above 20 Hz to 16 jobs for the band 10–20 Hz.

TABLE I. Number of surviving candidates at each stage of the veto chain. Double (HL, LV, HV) and triple (HLV) coincidences are done among candidates surviving the known lines removal. For the HL pairs all the candidates above the CR threshold are followed up, while for the LV and HV pair we do not follow up candidates above 100 Hz. For the HLV case there were only two candidates with $\rho_{\mathrm{CR}}(n) > \rho_{\mathrm{CR,thr}}$, hence we also follow up the only candidate present below 100 Hz even if its significance is below the threshold. A total of 361 candidates passed to the next step of the analysis described in Sec. IV B.

	Single	After lines removal	
H	3409029	3135640	
L	3410398	3250804	
V	3408485	3240966	
	Double	$f_0 < 100$ Hz	$\rho_{\mathrm{CR}}(n) > \rho_{\mathrm{CR,thr}}$
HL	37570	Selection not applied	274
LV	37455	458	40
HV	36988	381	44
	Triple		
HLV	2142	1	2

The list of instrumental artifacts for which the source is not completely understood (e.g., unknown lines) are not used to veto candidates at this stage of the search.

For the consistency veto [34,64] we have discarded all coincident candidates that show a weighted CR in the less sensitive detector more than 3 times higher than the one in the more sensitive detector. At this stage the CR we are considering is the one computed from the FH number count. At a later stage, a second consistency veto will be applied using the 5n-vector $\mathcal{S}$-statistic [65,66] (see Sec. IV B). In practice, assuming that the noise spectral density in the first detector is worse, i.e., $S_{n_1}(f) > S_{n_2}(f)$, only the outliers with $\rho_{\mathrm{CR}_1}/\sqrt{S_{n_1}(f)} < 3\rho_{\mathrm{CR}_2}/\sqrt{S_{n_2}(f)}$ survive to the next postprocessing step. In this search, however, this veto only had a very minor effect, removing only one candidate in the HL pair when applied after the lines veto.

About 37000 outliers survived after the cuts for the double coincidences HL, LV, and HV, while only ∼2000 coincident outliers did pass this first selection for the triple coincidence case (HLV). Exact numbers are reported in Table I. As discussed at the end of Sec. III B, we further reduce the number of candidates to pass to the next veto/follow-up stages according to their significance ρ_{CR} and/or if their frequencies are below 100 Hz (see Table I).

B. Semicoherent 5n-vector follow-up

On the double- and triple-coincident outliers passing the previous vetoes, we have applied a semicoherent follow-up method, based on the so-called "5n-vectors," already used in [27], which will be briefly summarized here. The method is based on the expected increase of the significance of a given outlier after the frequency modulations are removed from the data, e.g., by applying the heterodyne correction. For searches of CW signals from known pulsars, after removing the effects that modulate the frequency, an amplitude modulation—due to the sidereal pattern—still remains. The sidereal modulation pattern, that arises when the signal is integrated for a chunk of data at least equal to the sidereal day, is the key ingredient used to distinguish between an astrophysical signal or a noise outlier. This modulation produces a splitting of the intrinsic signal angular frequency ω_0 into five frequencies $\omega_0, \omega_0 \pm \Omega_{\mathrm{sid}}, \omega_0 \pm 2\Omega_{\mathrm{sid}}$, where Ω_{sid} is Earth's sidereal angular frequency.

The 5n-vector template is then built assuming as known the frequency, spin down, and sky position of the source. In our case we apply a matched filter using the 5n-vector shape to chunks of data with duration $T_{\mathrm{sid}} = 2\pi/\Omega_{\mathrm{sid}}$ equal to one sidereal day, and a final detection statistic $\mathcal{S}$ is computed summing all the detection statistics computed in each chunk. The same calculation is done in the off-source region, i.e., away from the frequency of the candidate. Details on the $\mathcal{S}$-statistic can be found in [27]. From the $\mathcal{S}$-statistic it is possible to compute the corresponding CR and signal-to-noise ratio values.

We compute the significance of a given outlier using the semicoherent method described above in two different situations: (i) when we remove the Doppler and spin-down modulations (in this case, if the outlier is of astrophysical origin we expect to have a higher significance) and (ii) when no demodulation is applied to the time series. We expect to have an increase of the significance for the case of the demodulated signal when compared to the case where no demodulation is applied. We use these criteria to keep interesting outliers and pass them to the final follow-up stage. After this stage the number of remaining candidates decrease to 62 for the HL pair, 13 and 10 for the HV and LV pairs with frequencies below 100 Hz, respectively. Two out of the three HLV candidates investigated in this stage have been discarded, while the candidate below 100 Hz passed to the next step.

C. Cumulative significance check

For this follow-up stage we rely on the consistency of the significance of a CW signal during the observing time. Specifically, we expect that the significance of a signal will steadily increase as we integrate over more time and hence accumulate more power, following a positive trend as more data are used. On the other hand, a sudden increase or decrease in the significance as more data are integrated is a clue indicating the presence of nonstationary noise. We compute the cumulative signal-to-noise ratio and CR on a monthly basis using the 5n-vector statistic over a starting time series (no Doppler or spin-down phase correction is applied), and we compare this trend with the one using the heterodyne-corrected time series. The heterodyne phase

correction applied in this latter case, $e^{i\phi(f_0,\dot{f}_0)}$, is fully described by the parameters of the outlier investigated. These curves are computed separately for each detector. Many outliers presented inconsistencies between the corrected vs the uncorrected case in the same detector (e.g., the cumulative curve of the uncorrected case was always above the corresponding corrected one) or inconsistencies between the two detectors (e.g., for the corrected time series, the cumulative curve of the less sensitive detector was always above the corresponding curve of the most sensitive one). The inconsistencies between the curves suggest that these outliers have been produced by an artifact in only one detector. Indeed for the HV and LV pairs and the HLV triplets, all of the outliers have been discarded with this veto, while 15 candidates for the HL pair were further investigated through visual inspection. We describe these additional tests in the following.

D. Spectra and peak maps inspection

To further investigate the remaining 15 outliers from HL, we visually inspect the spectra and the peak maps using different frequency resolutions. In this way eventually hidden noise features can arise, e.g., narrower spectral lines, and the true origin of the signal candidate can be found. As a second check we have verified if some of the remaining outliers had an evolving frequency that crossed one of the lines of the unidentified set of spectral noise artifacts found in the detectors [67], although none of the candidates overlapped with this set of unidentified lines. Concerning the spectra we have visually inspected differences and similarities between (i) the spectra of the heterodyned time series, corrected using the candidate's parameters $(f_0, \dot{f}_0)$, and (ii) the original spectra, when no correction is applied. If instrumental lines are present these should be present also before correcting the time series. We use three different frequency resolutions for these spectra of 3.2×10^{-8}, 3.2×10^{-7}, and 3.2×10^{-6} Hz, equivalent to full resolution spectra (12 months, full run, no average) and to averaging over chunks of duration $T_{\mathrm{obs}}/10$, $T_{\mathrm{obs}}/100$, respectively. Concerning the peak maps, we have checked if local maxima appear in the frequency histogram of the peak maps (i.e., the peak map projected onto the frequency axis) in the corrected and/or uncorrected case. Also in this case, if an instrumental line is present, this should appear in the peak map and peak map histogram before correction, polluting the interested band. These peak maps have a frequency resolution of $1/T_{\mathrm{coh}}$ while the histograms are built using five different bin widths from $1/T_{\mathrm{coh}}$ to $5/T_{\mathrm{coh}}$. We use wider bins to be robust against signals which may deviate from the model (or if the candidate's parameters are not accurate enough). Through this inspection we have been able to discard 13 out of these 15 candidates, given the presence of noise spectral artifacts likely consistent with weak instrumental lines in the frequency band intersected by the candidate, which clearly appear either in the uncorrected spectra or in the peak map histograms.

TABLE II. Parameters of the surviving outlier. The sky position is the one used for the search and coincident to that of Sgr A* with $\alpha_{\mathrm{GC}} = 17$ h 45 m 40.04 s and $\delta_{\mathrm{GC}} = -29°00' 28.1''$. The reference time for the parameters is 1238112018 GPS.

Detector	f_0 (Hz)	$\dot{f}_0$ (Hz/s)	$\rho_{\mathrm{CR}}(n)$
H	908.7708738	-2.511×10^{-9}	5.17
L	908.7704061	-2.521×10^{-9}	4.99

Two out of these 15 visually inspected candidates did not show a clear presence of a weak line nearby before correction, although neither a strong feature suggesting their astrophysical origin after the correction (e.g., a typical 5n-vector shape in the corrected spectra). We quantify the significance associated with these candidates using the peak map histogram counts over the frequency. We consider the frequency subband originally used to select the candidates in the FrequencyHough map. We divide this 0.01-Hz band into subbands of 5 bins each. Over each of these smaller frequency subbands we pick the maximum count of the peak map projection. We then compare the position of the maximum peak map histogram count of the candidate subband with all the maxima computed on the remaining subbands.

We tag as interesting the candidates ranking first or second among the subbands in both detectors. One of the two surviving candidates ranked 59th in H and 30th in L, hence we discard it.

The second candidate ranked 11th in H and first in L, thus confirming its low significance in the Hanford detector. We ran an additional complementary multistage follow-up using the method described in [68] with the PyFstat package [69,70] and with the same configuration as in [64]. The resulting Bayes factor was significantly lower than what would be expected for a signal within the probed sensitivity range. The original parameters of the candidates are reported in Table II. Also, the initial threshold used for candidate selection was extremely low, opening the possibility to select such outliers compatible with noise fluctuations. As there is no strong evidence for the presence of an astrophysical signal, we can compute upper limits on the signal strain and from them derive some astrophysical constraints.

V. RESULTS

In this section we present the estimates of the upper limits on the signal strain and the constraints we can place in the absence of a detection. We use a quick method to estimate the upper limits, i.e., the maximum h_0 allowed by this search, above which we can exclude the presence of a CW signal with a given confidence level (CL). These limits can be translated into some astrophysical constraints on the

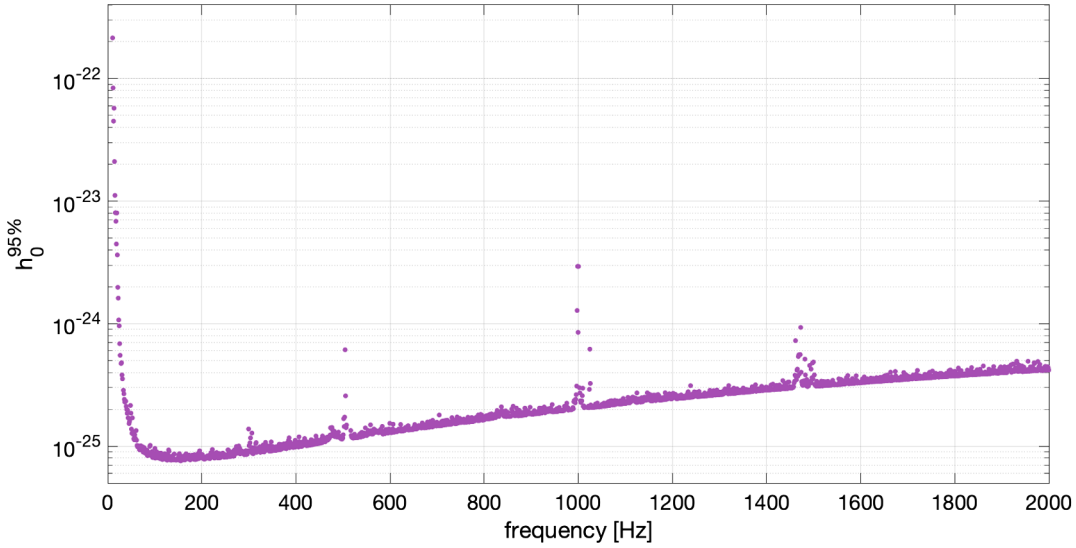

FIG. 2. Estimates of the 95% CL strain upper limits, derived for the best combination HL in 1-Hz bands [72].

ellipticity of neutron stars and the r-mode amplitude. Furthermore, we present for the first time—for a directed search toward the GC—"exclusion regions" for the boson mass and black hole mass for boson clouds forming around spinning black holes.

A. Upper limits

We provide an estimate of the upper limits using a method based on the sensitivity estimates presented in [58]. The minimum detectable strain amplitude $h_{0,\mathrm{min}}$, with $\Gamma = 0.95$ corresponding to a 95% CL, can be written as

$$h_{0,\mathrm{min}} \approx \frac{\mathcal{B}}{N^{1/4}} \sqrt{\frac{S_n(f)}{T_{\mathrm{coh}}}} \sqrt{\rho_{\mathrm{CR,thr}} - \sqrt{2} erfc^{-1}(2\Gamma)}, \quad (7)$$

where $N \sim T_{\mathrm{obs}}/T_{\mathrm{coh}}$ is the effective number of fast Fourier transforms used for the search. In this equation, $\mathcal{B}$ is a parameter that depends on the threshold used for peak selection in the peak map and on a factor dependent on the sky position of the source and on the signal polarization, which is averaged out. For this search we have computed the value of $\mathcal{B}$ for the GC case. More details are provided in the Appendix. The formula in Eq. (7) expresses the minimum detectable strain by a search which selects the candidate with a CR higher than $\rho_{\mathrm{CR,thr}}$, i.e., it states the best sensitivity a given search can achieve when the minimum CR of our candidates coincides with $\rho_{\mathrm{CR,thr}}$. On the other hand, if we want to look for the maximum allowed h_0, above which we can exclude the presence of a CW signal, i.e., provide an estimate of the upper limit, we can substitute for $\rho_{\mathrm{CR,thr}}$ the value of the maximum CR ($\rho_{\mathrm{CR,max}}$) found in a given frequency band. The width of the 1-Hz frequency band determines the resolution of the upper limits estimate.

We have verified that this estimate of the upper limits, using $\rho_{\mathrm{CR,max}}$ in Eq. (7), already implemented in [64,71], indeed yields conservative limits if compared to the results obtained with the classical frequentist approach using artificially injected signals. This check has been performed on six frequency bands of 1 Hz each, randomly chosen over the full frequency range investigated. We have also verified that the 95% CL upper limits, obtained using software injected signals, are always above the curve defined in Eq. (7) when $\rho_{\mathrm{CR,thr}}$ is used. Furthermore, the difference between the upper limits obtained using injections and those computed using this method is still within the calibration uncertainty errors, which are already affecting the estimate of the noise power spectral density $S_n(f)$ (see Sec. II [51–53]).

The curve shown in Fig. 2 represents the joint upper limits estimate of the coincident pair HL. This is obtained by computing the $h_0^{95\%}(\rho_{\mathrm{CR,max}}, S_n)$ separately for each H and L detector and keeping the worst of the two curves in each Hz. For a given detector, the CR has been taken equal to the maximum in each 1-Hz band, otherwise was set equal to $\rho_{\mathrm{CR,thr}}$ if the maximum CR in that band was lower than $\rho_{\mathrm{CR,thr}}$. Given that for a given pair (or triplet) of detectors the combined upper limits curves are dominated by the less sensitive detector, we do not report the LV, HV, HLV associated curves given the large difference between the $S_n(f)$ of the Virgo detector compared to the power spectral density of Hanford and Livingston. From the curve in Fig. 2 it is possible to see a minimum strain of $\sim 7.6 \times 10^{-26}$ at 140 Hz. This result improves on the one in [34] using O2 data by a factor $\simeq 1.9$.

B. Astrophysical implications

We can exploit the relation between the GW strain amplitude and some astrophysical parameters characterizing

the emitting system to derive some constraints. In particular, for the isolated neutron star case, we can map the $h_0^{95\%}$ upper limit curve to a constraint on the ellipticity of the star [37], making some assumptions on the moment of inertia of the spinning star. It is also possible to convert the upper limits on the strain into constraints on the r-mode amplitude as discussed in [73], assuming a coherent emission during the observing time. In addition to these classic limits, typically derived for CW searches from neutron stars, we can derive some exclusion regions over the masses involved in a superradiance process of boson particles around spinning black holes as discussed in Sec. V B 2.

1. Neutron stars

Ellipticity.—For the prototypical case of a rotating neutron star with nonaxisymmetric deformations misaligned with the rotation axis, the strain amplitude is proportional to twice its spin frequency, $f_{\mathrm{GW}} = 2f_{\mathrm{spin}}$. This scenario corresponds, e.g., to the presence of mountains on the neutron star's surface [74] and the strain amplitude can be written as

$$h_0 = \frac{4\pi^2 G}{c^4}\frac{I_{zz} f_{\mathrm{GW}}^2}{d}\epsilon. \tag{8}$$

Assuming that the moment of inertia for a perpendicular biaxial rotor spinning around z, $I_{zz} = qI_{\mathrm{fid}}$, can be a multiple of the fiducial moment of inertia $I_{\mathrm{fid}} = 10^{38}\ \mathrm{kg\,m^2}$, where q is a proportionality factor,[3] the h_0 can be used to express the ellipticity of the neutron star as a function of the GW signal frequency and the moment of inertia as

$$\epsilon = 7 \times 10^{-4}\left(\frac{I_{\mathrm{fid}}}{I_{zz}}\right)\left(\frac{h_0}{10^{-24}}\right)\left(\frac{100\ \mathrm{Hz}}{f_{\mathrm{GW}}}\right)^2. \tag{9}$$

Here a distance of the GC of $d = 8$ kpc has been assumed, although different estimates of d exist [75–78]. In Fig. 3 we report the estimated 95% CL upper limits of the ellipticity, $\epsilon^{95\%}$. The two curves indicate the two extreme cases for $I_{zz} = I_{\mathrm{fid}}$ (upper curve), and $I_{zz} = 5I_{\mathrm{fid}}$ (lower curve). The shaded region spans all the possibilities between the $q = 1$ and $q = 5$ case. Moments of inertia 5 times larger than the fiducial value can possibly be sustained by stars made up of more exotic components. For the $q = 1$ case the minimum ellipticity reached for the highest frequency is $\epsilon = 7.26 \times 10^{-7}$, while a minimum of $\epsilon = 1.45 \times 10^{-7}$ is obtained for the $q = 5$ case. Given this high uncertainty of the actual moment of inertia of the star (dependent on both the mass and the radius of the star), it is useful to quote the corresponding mass quadrupole Q_{22}

[3]The exact value of a neutron star's moment of inertia is unknown and it strongly depends on its EOS; for this reason we will use a proportionality factor $q = 1$ (normal matter) and $q = 5$ (extreme matter) to cover these two extremes, see [37].

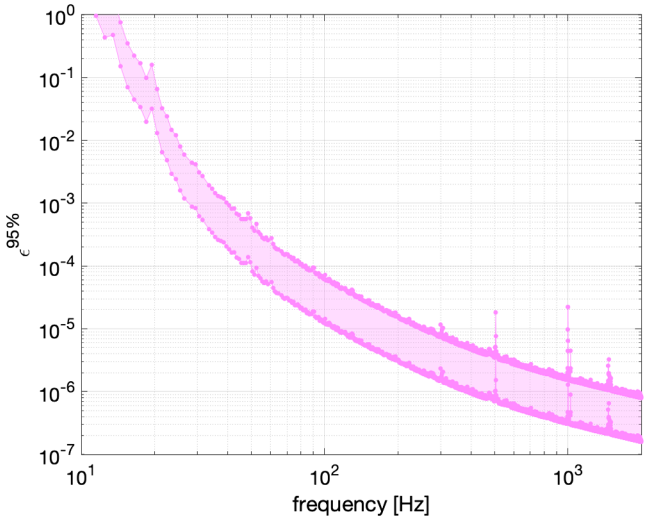

FIG. 3. Estimates of the 95% CL ellipticity upper limits assuming a GC distance of 8 kpc. The shaded area between the two curves covers the possible values of the moment of inertia along z of the spinning star. The lower curve corresponds to a moment of inertia 5 times larger than the fiducial value I_{fid}, sustainable by exotic objects.

component of the $l = m = 2$ mode, which is present in the expression of the GW amplitudes in the mass quadrupole formalism [79]

$$Q_{22} = \sqrt{\frac{15}{8\pi}}\epsilon I_{zz}. \tag{10}$$

This quantity is then independent of the actual moment of inertia used and is directly connected with h_0 [see Eq. (8)]. A minimum value of $Q_{22} = 5.61 \times 10^{31}\ \mathrm{kg\,m^2}$ is reached at the highest frequency.

In this simplest model we are not considering the possible multiple harmonic emission mechanism active in situations like a superfluid pinned to the crust, a triaxial star not spinning around its principal axis, and more [80,81], where additional radiation is expected at the star's spin frequency f_{spin} as well at the $2f_{\mathrm{spin}}$ frequency. The case of free precession would require including further terms in addition to the dual harmonic components [82].

R-mode amplitude.—Changing the emission scenario but still staying in the single harmonic emission model, the limits on the strain can be parametrized for the case of unstable oscillation modes, namely r-modes, happening at $f_{\mathrm{GW}} = \frac{4}{3}f_{\mathrm{spin}}$ in the nonrelativistic case. The actual proportionality factor between f_{spin} and f_{GW} is expected to differ from $\frac{4}{3}$ in the relativistic case and when the EOS dependence is considered (see [83,84]).

Following the discussion in [73] it is possible to convert upper limits from the "mountain" scenario to the equivalent

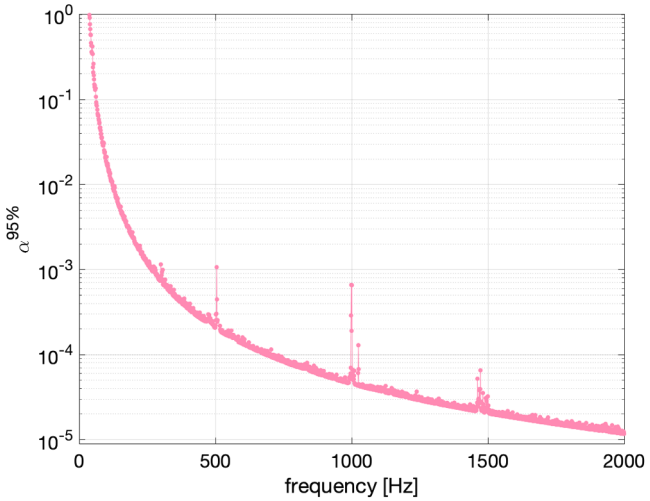

FIG. 4. Estimates of the 95% CL r-mode amplitude upper limits for neutron stars in the GC region assuming $d = 8$ kpc.

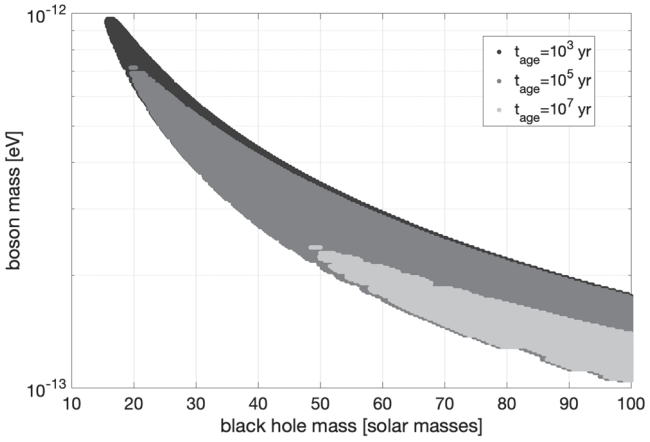

FIG. 5. Constraints on the black hole mass–boson mass plane, assuming CW emission from boson clouds around spinning black holes located in the GC. An initial black hole dimensionless spin $\chi_i = 0.5$ and cloud ages of $t_{\rm age} = 10^3, 10^5, 10^7$ yr are considered. The reported exclusion regions have been derived from the upper limits in [72].

r-mode expression, given that the latter can be obtained from the standard expression in the ellipticity case through the mapping $\psi \to \psi + \pi/4$ corresponding to a 45° rotation of the polarization angle ψ. The amplitude of r-mode emissions is then given by

$$\alpha \simeq 0.028 \left(\frac{h_0}{10^{-24}}\right)\left(\frac{d}{1\ \text{kpc}}\right)\left(\frac{100\ \text{Hz}}{f_{\rm GW}}\right)^3. \quad (11)$$

This equation has been obtained assuming the dimensionless functional of the neutron star EOS $\tilde{J} \approx 0.0164$ and a neutron star with mass $M = 1.4\ M_\odot$ and radius R = 11.7 km as in [73]. We report the converted 95% CL upper limits on the r-mode amplitude α in Fig. 4, assuming a GC distance of 8 kpc as done for Fig. 3. Minimum values of $\alpha \sim 10^{-5}$ are reached for the highest frequencies.

2. Boson clouds

A population of thousands of stellar-mass black holes is expected to exist near the GC [85] and observational evidence is accumulating, see, e.g., [86,87]. A fraction of these black holes may have developed a boson cloud [42–45,48] which is currently depleting by emitting CWs.

In order to put constraints on the boson cloud systems we have first derived the upper limits curve in Fig. 2, using only candidates with a positive spin down (e.g., with spin up). This is a necessary step to have a more accurate estimate to use for our constraints, since the signal produced by boson clouds around spinning black holes is characterized by a spin up [42] and no spin down is expected as for the case of spinning neutron stars.

Given an upper limits curve, we can translate it into constraints in the black hole/boson mass parameter space. Following what was done in previous all-sky searches [71,88], we compute exclusion regions in the parameter space for a given value of the black hole spin before the superradiant cloud growth χ_i and for different boson cloud ages, $t_{\rm age}$. The distance is fixed to 8 kpc. Specifically, Fig. 5 shows the constraints for $\chi_i = 0.5$ and $t_{\rm age} = 10^3, 10^5$, and 10^7 yr. Going from these constraints, valid for specific parameter choices, to the actual exclusion of given combinations of black hole and boson masses is not trivial, as it depends on the uncertain characteristics of the black hole population in the GC. In particular, it is expected that many black holes now residing in the GC region may have ages of gigayears [89] and then would not be relevant anymore from the CW emission point of view. On the other hand, a non-negligible number of black holes should have formed more recently, both by core collapse of a progenitor massive star or by the coalescence of black hole binary systems, formed, e.g., by tidal capture in the dense GC environment [90]. These systems could have developed a boson cloud which is still in the CW emission phase. A quantitative study of this subject is clearly important but outside the scope of the current paper.

VI. CONCLUSION

We have presented a search for continuous GWs from sources in the GC using LIGO and Virgo data from the third observing run. Although the core of this search is the same as the one presented in [34], a more sensitive, longer dataset has been used, and several novelties have been introduced in this version. First of all the parameter space investigated is much wider, allowing for high-frequency emitters to be searched for. In addition, data from the Virgo detector has been used for the first time, providing an increased number of potential candidates. Along with these extensions, new techniques have been applied in the follow-up part and for

the computation of upper limits. The enormous reduction of the computational load of this last step of the analysis allows for a better use of the resources in the follow-up part. Indeed this makes possible the use of a lower threshold in the first pass selection of candidates, increasing the final number of outliers, the chance of detection, and the overall search sensitivity. One marginal outlier near 909 Hz (see Table II) could not be decisively ruled out, but is more consistent with a single-detector noise fluctuation.

The deepest strain limit is 7.6×10^{-26} at 142 Hz, corresponding to levels of ellipticity well below the maximum value expected for a neutron star composed of standard matter [37,91,92], solid strange stars, or hybrid and meson-condensate stars [79] for most of the frequency band investigated. The most stringent constraints on the r-mode amplitude are obtained at the highest frequencies well below expected quantities for the nonlinear saturation mechanisms [93]. Finally we provide new constraints on the mass distribution of boson cloud masses in addition to those presented in [71].

ACKNOWLEDGMENTS

This material is based upon work supported by NSF's LIGO Laboratory which is a major facility fully funded by the National Science Foundation. The authors also gratefully acknowledge the support of the Science and Technology Facilities Council (STFC) of the United Kingdom, the Max-Planck-Society (MPS), and the State of Niedersachsen/Germany for support of the construction of Advanced LIGO and construction and operation of the GEO 600 detector. Additional support for Advanced LIGO was provided by the Australian Research Council. The authors gratefully acknowledge the Italian Istituto Nazionale di Fisica Nucleare (INFN), the French Centre National de la Recherche Scientifique (CNRS), and the Netherlands Organization for Scientific Research (NWO), for the construction and operation of the Virgo detector and the creation and support of the EGO consortium. The authors also gratefully acknowledge research support from these agencies as well as by the Council of Scientific and Industrial Research of India, the Department of Science and Technology, India, the Science and Engineering Research Board (SERB), India, the Ministry of Human Resource Development, India, the Spanish Agencia Estatal de Investigación (AEI), the Spanish Ministerio de Ciencia e Innovación and Ministerio de Universidades, the Conselleria de Fons Europeus, Universitat i Cultura and the Direcció General de Política Universitaria i Recerca del Govern de les Illes Balears, the Conselleria d'Innovació, Universitats, Ciència i Societat Digital de la Generalitat Valenciana, and the CERCA Programme Generalitat de Catalunya, Spain, the National Science Centre of Poland and the European Union—European Regional Development Fund; Foundation for Polish Science (FNP), the Swiss National Science Foundation (SNSF), the Russian Foundation for Basic Research, the Russian Science Foundation, the European Commission, the European Social Funds (ESF), the European Regional Development Funds (ERDF), the Royal Society, the Scottish Funding Council, the Scottish Universities Physics Alliance, the Hungarian Scientific Research Fund (OTKA), the French Lyon Institute of Origins (LIO), the Belgian Fonds de la Recherche Scientifique (FRS-FNRS), Actions de Recherche Concertées (ARC), and Fonds Wetenschappelijk Onderzoek —Vlaanderen (FWO), Belgium, the Paris Île-de-France Region, the National Research, Development and Innovation Office Hungary (NKFIH), the National Research Foundation of Korea, the Natural Science and Engineering Research Council Canada, Canadian Foundation for Innovation (CFI), the Brazilian Ministry of Science, Technology, and Innovations, the International Center for Theoretical Physics South American Institute for Fundamental Research (ICTP-SAIFR), the Research Grants Council of Hong Kong, the National Natural Science Foundation of China (NSFC), the Leverhulme Trust, the Research Corporation, the Ministry of Science and Technology (MOST), Taiwan, the U.S. Department of Energy, and the Kavli Foundation. The authors gratefully acknowledge the support of the NSF, STFC, INFN, and CNRS for provision of computational resources. This work was supported by MEXT, JSPS Leading-edge Research Infrastructure Program, JSPS Grant-in-Aid for Specially Promoted Research 26000005, JSPS Grant-in-Aid for Scientific Research on Innovative Areas 2905: JP17H06358, JP17H06361, and JP17H06364, JSPS Core-to-Core Program A. Advanced Research Networks, JSPS Grant-in-Aid for Scientific Research (S) 17H06133 and 20H05639, JSPS Grant-in-Aid for Transformative Research Areas (A) 20A203: JP20H05854, the joint research program of the Institute for Cosmic Ray Research, University of Tokyo, National Research Foundation (NRF), Computing Infrastructure Project of KISTI-GSDC, Korea Astronomy and Space Science Institute (KASI), and Ministry of Science and ICT (MSIT) in Korea, Academia Sinica (AS), AS Grid Center (ASGC), and the Ministry of Science and Technology (MoST) in Taiwan under grants including AS-CDA-105-M06, Advanced Technology Center (ATC) of NAOJ, and Mechanical Engineering Center of KEK.

APPENDIX: DETAILS ON UPPER LIMITS FORMULA

Following the computation of Eq. (67) in [58] we want to compute the average prefactor $\mathcal{B}$ in Eq. (7) of this paper. The corresponding expression for $\mathcal{B}$ for the all-sky case described in [58] is equal to

$$\mathcal{B}_{\mathrm{all-sky}} = \frac{4.02}{\theta_{\mathrm{thr}}^{1/2}} \left(\frac{p_0(1-p_0)}{p_1^2} \right)^{1/4}, \tag{A1}$$

where the number 4.02 results from the average of all the varying quantities α, δ, and ψ [see Eq. (B19) in [58]]. All the remaining quantities, i.e., the peak selection threshold $\theta_{\rm thr} = 2.5$, the probability to select a noise peak $p_0 = 0.0755$, as well $p_1 = 0.0692$, a function depending on $\theta_{\rm thr}$, remain unchanged from [58] in this search. For our problem we need to evaluate the expression for a particular sky position and no averaging over α and δ is needed. On the other hand, we do need to average over time and the polarization parameter ψ, which is uniformly distributed over $[-\pi/4, \pi/4]$. Let us now consider the expressions for the beam pattern functions F_+ and $F_\times$ [94]

$$F_+(\psi, t) = a(t)\cos 2\psi + b(t)\sin 2\psi,$$
$$F_\times(\psi, t) = b(t)\cos 2\psi - a(t)\sin 2\psi. \tag{A2}$$

It is easy to check that the squared average over the polarization angle ψ is equal to 0.5. Hence we can write the squared average of F_+ and $F_\times$ as

$$\langle F_+^2\rangle_{\psi,t} = \langle F_+^2\rangle_{\psi,t} = \frac{1}{2}(\langle a^2\rangle_t + \langle b^2\rangle_t). \tag{A3}$$

Removing also the dependency over time and considering the following average expressions for $a^2(t)$ and $b^2(t)$ evaluated for the case $T_{\rm obs} = n2\pi/\Omega_{\rm sid}$, i.e., an integer number of sidereal days [95]:

$$\begin{aligned}\langle a^2\rangle_t &= \frac{1}{16}\sin^2 2\gamma\left[9\cos^4\phi\cos^4\delta + \frac{1}{2}\sin^2 2\phi\right.\\ &\left.\times \sin^2 2\delta + \frac{1}{32}(3-\cos 2\phi)^2(3-\cos 2\delta)^2\right]\\ &+ \frac{1}{32}\cos^2 2\gamma[4\cos^2\phi\sin^2 2\delta + \sin^2\phi(3-\cos 2\delta)^2],\\ \langle b^2\rangle_t &= \frac{1}{32}\sin^2 2\gamma[(3-\cos 2\phi)^2\sin^2\delta + 4\sin^2 2\phi\cos^2\delta]\\ &+ \frac{1}{4}\cos^2 2\gamma(1+\cos 2\phi\cos 2\delta).\end{aligned} \tag{A4}$$

Evaluating them for the specific sky location $\delta = \delta_{\rm GC}$ and for each (γ, ϕ) of a given detector, where ϕ is the latitude of the detector's site and γ is the orientation of the detector's arms, we can obtain different values for the antenna pattern functions per detector (i-det),

$$\begin{aligned}\langle F_+^2\rangle_{\psi,t}|_{\delta_{\rm GC},i-\rm det} &= \langle F_\times^2\rangle_{\psi,t}|_{\delta_{\rm GC},i-\rm det}\\ &= \frac{1}{2}(\langle a^2\rangle_t|_{\delta_{\rm GC},i-\rm det} + \langle b^2\rangle_t|_{\delta_{\rm GC},i-\rm det}).\end{aligned} \tag{A5}$$

The exact numbers entering as a prefactor of Eq. (67) of [58] for this search differ from the value used for the all-sky search in [58], where an average over the sky position is considered, by no more than the 3%. To be more accurate, the actual prefactors to be used in the calculation of our upper limits will be 4.06, 4.05, and 4.12 for H, L, and V, respectively, while for the all-sky case it is equal to 4.02. This means that $\mathcal{B}$ in Eq. (7) is equal to 5.06, 4.93, and 5.08 for H, L, and V, respectively, while it is equal to 4.97 for the all-sky case.

[1] K. M. Rajwade, D. R. Lorimer, and L. D. Anderson, Detecting pulsars in the Galactic Centre, Mon. Not. R. Astron. Soc. **471**, 730 (2017).
[2] C. Kim and M. B. Davies, Neutron stars in the Galactic Center, J. Korean Astron. Soc. **52**, 165 (2018).
[3] M. Ajello *et al.*, Fermi-LAT observations of high-energy γ-ray emission toward the Galactic Center, Astrophys. J. **819**, 44 (2016).
[4] M. Di Mauro, Characteristics of the Galactic Center excess measured with 11 years of Fermi-LAT data, Phys. Rev. D **103**, 063029 (2021).
[5] H. E. S. S. Collaboration, Acceleration of petaelectronvolt protons in the Galactic Centre, Nature (London) **531**, 476 (2016).
[6] A. Cuoco, M. Krämer, and M. Korsmeier, Novel Dark Matter Constraints from Antiprotons in Light of AMS-02, Phys. Rev. Lett. **118**, 191102 (2017).
[7] M.-Y. Cui, Q. Yuan, Y.-L. S. Tsai, and Y.-Z. Fan, Possible Dark Matter Annihilation Signal in the AMS-02 Antiproton Data, Phys. Rev. Lett. **118**, 191101 (2017).
[8] A. Albert *et al.*, Searching for dark matter annihilation in recently discovered Milky Way satellites with Fermi-LAT, Astrophys. J. **834**, 110 (2017).
[9] M. Ackermann *et al.*, The Fermi Galactic Center GeV excess and implications for dark matter, Astrophys. J. **840**, 43 (2017).
[10] M. Di Mauro and M. W. Winkler, Multimessenger constraints on the dark matter interpretation of the Fermi-LAT Galactic Center excess, Phys. Rev. D **103**, 123005 (2021).
[11] R. Bartels, S. Krishnamurthy, and C. Weniger, Strong Support for the Millisecond Pulsar Origin of the Galactic Center GeV Excess, Phys. Rev. Lett. **116**, 051102 (2016).
[12] S. K. Lee, M. Lisanti, B. R. Safdi, T. R. Slatyer, and W. Xue, Evidence for Unresolved γ-Ray Point Sources in the Inner Galaxy, Phys. Rev. Lett. **116**, 051103 (2016).
[13] F. Calore, M. Di Mauro, F. Donato, J. W. T. Hessels, and C. Weniger, Radio detection prospects for a bulge population of millisecond pulsars as suggested by FERMI-LAT observations of the inner galaxy, Astrophys. J. **827**, 143 (2016).

[14] T. Grégoire and J. Knödlseder, Constraining the Galactic millisecond pulsar population using Fermi Large Area Telescope, Astron. Astrophys. **554**, A62 (2013).
[15] Fermi-LAT Collaboration, Characterizing the population of pulsars in the inner Galaxy with the Fermi Large Area Telescope, arXiv:1705.00009.
[16] D. Hooper and T. Linden, Millisecond pulsars, TeV halos, and implications for the Galactic Center gamma-ray excess, Phys. Rev. D **98**, 043005 (2018).
[17] M. Buschmann, N. L. Rodd, B. R. Safdi, L. J. Chang, S. Mishra-Sharma, M. Lisanti, and O. Macias, Foreground mismodeling and the point source explanation of the Fermi Galactic Center excess, Phys. Rev. D **102**, 023023 (2020).
[18] T. Lacroix, J. Silk, E. Moulin, and C. Bœhm, Connecting the new H. E. S. S. diffuse emission at the Galactic Center with the Fermi GeV excess: A combination of millisecond pulsars and heavy dark matter?, Phys. Rev. D **94**, 123008 (2016).
[19] O. J. Piccinni, Status and perspectives of continuous gravitational wave searches, Galaxies **10**, 72 (2022).
[20] K. Riles, Searches for continuous-wave gravitational radiation, arXiv:2206.06447.
[21] K. Riles, Recent searches for continuous gravitational waves, Mod. Phys. Lett. A **32**, 1730035 (2017).
[22] M. Sieniawska and M. Bejger, Continuous gravitational waves from neutron stars: Current status and prospects, Universe **5**, 217 (2019).
[23] R. Abbott *et al.*, Gravitational-wave constraints on the equatorial ellipticity of millisecond pulsars, Astrophys. J. Lett. **902**, L21 (2020).
[24] R. Abbott *et al.*, All-sky search in early O3 LIGO data for continuous gravitational-wave signals from unknown neutron stars in binary systems, Phys. Rev. D **103**, 064017 (2021).
[25] R. Abbott *et al.*, Diving below the spin-down limit: Constraints on gravitational waves from the energetic young pulsar PSR J0537-6910, Astrophys. J. Lett. **913**, L27 (2021).
[26] R. Abbott *et al.*, Constraints from LIGO O3 data on gravitational-wave emission due to r-modes in the glitching pulsar PSR J0537-6910, Astrophys. J. **922**, 71 (2021).
[27] R. Abbott *et al.*, Searches for continuous gravitational waves from young supernova remnants in the early third observing run of advanced LIGO and Virgo, Astrophys. J. **921**, 80 (2021).
[28] R. Abbott *et al.*, All-sky search for continuous gravitational waves from isolated neutron stars in the early O3 LIGO data, Phys. Rev. D **104**, 082004 (2021).
[29] R. Abbott *et al.* (LIGO Scientific Collaboration, Virgo Collaboration, and KAGRA Collaboration), Search for continuous gravitational waves from 20 accreting millisecond X-ray pulsars in O3 LIGO data, Phys. Rev. D **105**, 022002 (2022).
[30] R. Tenorio, D. Keitel, and A. M. Sintes, Search methods for continuous gravitational-wave signals from unknown sources in the advanced-detector era, Universe **7**, 474 (2021).
[31] F. Acernese *et al.*, Advanced Virgo: A second-generation interferometric gravitational wave detector, Classical Quantum Gravity **32**, 024001 (2015).
[32] J. Aasi *et al.*, Advanced LIGO, Classical Quantum Gravity **32**, 074001 (2015).
[33] O. J. Piccinni, P. Astone, S. D'Antonio, S. Frasca, G. Intini, P. Leaci, S. Mastrogiovanni, A. Miller, C. Palomba, and A. Singhal, A new data analysis framework for the search of continuous gravitational wave signals, Classical Quantum Gravity **36**, 015008 (2019).
[34] O. J. Piccinni, P. Astone, S. D'Antonio, S. Frasca, G. Intini, I. La Rosa, P. Leaci, S. Mastrogiovanni, A. Miller, and C. Palomba, Directed search for continuous gravitational-wave signals from the galactic center in the advanced LIGO second observing run, Phys. Rev. D **101**, 082004 (2020).
[35] R. Abbott *et al.*, Search for anisotropic gravitational-wave backgrounds using data from advanced LIGO's and advanced Virgo's first three observing runs, Phys. Rev. D **104**, 022005 (2021).
[36] K. Glampedakis and L. Gualtieri, Gravitational waves from single neutron stars: An advanced detector era survey, Astrophysics and Space Science Library **457**, 673 (2018).
[37] N. K. Johnson-McDaniel and B. J. Owen, Maximum elastic deformations of relativistic stars, Phys. Rev. D **88**, 044004 (2013).
[38] J. M. Lattimer, The physics of neutron stars, Science **304**, 536 (2004).
[39] N. Andersson, A new class of unstable modes of rotating relativistic stars, Astrophys. J. **502**, 708 (1998).
[40] L. Bildsten, Gravitational radiation and rotation of accreting neutron stars, Astrophys. J. **501**, L89 (1998).
[41] J. L. Friedman and S. M. Morsink, Axial instability of rotating relativistic stars, Astrophys. J. **502**, 714 (1998).
[42] A. Arvanitaki, M. Baryakhtar, and X. Huang, Discovering the QCD axion with black holes and gravitational waves, Phys. Rev. D **91**, 084011 (2015).
[43] M. Baryakhtar, M. Galanis, R. Lasenby, and O. Simon, Black hole superradiance of self-interacting scalar fields, Phys. Rev. D **103**, 095019 (2021).
[44] R. Brito, V. Cardoso, and P. Pani, Superradiance, Lect. Notes Phys. **971**, 1 (2020).
[45] R. Brito, S. Ghosh, E. Barausse, E. Berti, V. Cardoso, I. Dvorkin, A. Klein, and P. Pani, Gravitational wave searches for ultralight bosons with LIGO and LISA, Phys. Rev. D **96**, 064050 (2017).
[46] H. Yoshino and H. Kodama, The bosenova and axiverse, Classical Quantum Gravity **32**, 214001 (2015).
[47] W. E. East and F. Pretorius, Superradiant Instability and Backreaction of Massive Vector Fields around Kerr Black Holes, Phys. Rev. Lett. **119**, 041101 (2017).
[48] R. Brito and P. Pani, Black-hole superradiance: Searching for ultralight bosons with gravitational waves, in *Handbook of Gravitational Wave Astronomy*, edited by C. Bambi, S. Katsanevas, and K. D. Kokkotas (Springer Singapore, Singapore, 2020), pp. 1–33.
[49] C. A. R. Herdeiro and E. Radu, Dynamical Formation of Kerr Black Holes with Synchronized Hair: An Analytic Model, Phys. Rev. Lett. **119**, 261101 (2017).
[50] N. Siemonsen and W. E. East, Gravitational wave signatures of ultralight vector bosons from black hole superradiance, Phys. Rev. D **101**, 024019 (2020).

[51] L. Sun *et al.*, Characterization of systematic error in Advanced LIGO calibration, Classical Quantum Gravity **37**, 225008 (2020).
[52] L. Sun *et al.*, Characterization of systematic error in Advanced LIGO calibration in the second half of O3, arXiv:2107.00129.
[53] F. Acernese *et al.* (Virgo Collaboration), Calibration of Advanced Virgo and reconstruction of detector strain h(t) during the observing run O3, Classical Quantum Gravity **39**, 045006 (2022).
[54] J. Zweizig and K. Riles, Information on self-gating of h(t) used in O3 continuous-wave and stochastic searches, Techncal Report No. LIGO-T2000384, LIGO Laboratory, 2021.
[55] P. Astone, S. Frasca, and C. Palomba, The short FFT database and the peak map for the hierarchical search of periodic sources, Classical Quantum Gravity **22**, S1197 (2005).
[56] E. Goetz *et al.*, O3a lines and combs found in self-gated C01 data, Technical Report No. LIGO-T2100200, LIGO Laboratory, 2021.
[57] O. J. Piccinni, K. Janssens, I. Fiori, C. Palomba, K. Turbang, L. Pierini, M. C. Tringali, N. Arnaud, and A. Trovato, Virgo O3 list of lines, Technical Report No. LIGO-T2100141-v2 LIGO Laboratory, 2021.
[58] P. Astone, A. Colla, S. D'Antonio, S. Frasca, and C. Palomba, Method for all-sky searches of continuous gravitational wave signals using the frequency-hough transform, Phys. Rev. D **90**, 042002 (2014).
[59] A. Singh, M. A. Papa, and V. Dergachev, Characterizing the sensitivity of isolated continuous gravitational wave searches to binary orbits, Phys. Rev. D **100**, 024058 (2019).
[60] M. J. Reid and A. Brunthaler, The proper motion of sagittarius A*. III. The case for a supermassive black hole, Astrophys. J. **892**, 39 (2020).
[61] F. Antonucci, P. Astone, S. D'Antonio, S. Frasca, and C. Palomba, Detection of periodic gravitational wave sources by Hough transform in the f versus $\dot{f}$ plane, Classical Quantum Gravity **25**, 184015 (2008).
[62] D. Davis *et al.*, LIGO detector characterization in the second and third observing runs, Classical Quantum Gravity **38**, 135014 (2021).
[63] P. B. Covas *et al.*, Identification and mitigation of narrow spectral artifacts that degrade searches for persistent gravitational waves in the first two observing runs of advanced LIGO, Phys. Rev. D **97**, 082002 (2018).
[64] R. Abbott *et al.*, All-sky search for continuous gravitational waves from isolated neutron stars using Advanced LIGO and Advanced Virgo O3 data, arXiv:2201.00697.
[65] P. Astone, S. D'Antonio, S. Frasca, and C. Palomba, A method for detection of known sources of continuous gravitational wave signals in non-stationary data, Classical Quantum Gravity **27**, 194016 (2010).
[66] P. Astone, A. Colla, S. D'Antonio, S. Frasca, C. Palomba, and R. Serafinelli, Method for narrow-band search of continuous gravitational wave signals, Phys. Rev. D **89**, 062008 (2014).
[67] E. Goetz *et al.*, Unidentified O3 lines found in self-gated C01 data, Technical Report No. LIGO-T2100201, LIGO Laboratory, 2021.
[68] R. Tenorio, D. Keitel, and A. M. Sintes, Application of a hierarchical MCMC follow-up to Advanced LIGO continuous gravitational-wave candidates, Phys. Rev. D **104**, 084012 (2021).
[69] G. Ashton and R. Prix, Hierarchical multistage MCMC follow-up of continuous gravitational wave candidates, Phys. Rev. D **97**, 103020 (2018).
[70] D. Keitel, R. Tenorio, G. Ashton, and R. Prix, PyFstat: A Python package for continuous gravitational-wave data analysis, J. Open Source Softwaare **6**, 3000 (2021).
[71] R. Abbott *et al.*, All-sky search for gravitational wave emission from scalar boson clouds around spinning black holes in LIGO O3 data, Phys. Rev. D **105**, 102001 (2022).
[72] See Supplemental Material at http://link.aps.org/supplemental/10.1103/PhysRevD.106.042003 for numerical values of upper limits.
[73] B. J. Owen, How to adapt broad-band gravitational-wave searches for r-modes, Phys. Rev. D **82**, 104002 (2010).
[74] F. Gittins, N. Andersson, and D. I. Jones, Modelling neutron star mountains, Mon. Not. R. Astron. Soc. **500**, 5570 (2020).
[75] R. Abuter *et al.* (The GRAVITY Collaboration), A geometric distance measurement to the galactic center black hole with 0.3% uncertainty, Astron. Astrophys. **625**, L10 (2019).
[76] A. Eckart, A. Hüttemann, C. Kiefer, S. Britzen, M. Zajaček, C. Lämmerzahl, M. Stöckler, M. Valencia-S, V. Karas, and M. García-Marín, The Milky Way's supermassive black hole: How good a case is it?, Found. Phys. **47**, 553 (2017).
[77] C. Francis and E. Anderson, Two estimates of the distance to the Galactic Centre, Mon. Not. R. Astron. Soc. **441**, 1105 (2014).
[78] T. Hirota *et al.*, The first VERA astrometry catalog, Publ. Astron. Soc. Jpn. **72**, 50 (2020).
[79] B. J. Owen, Maximum Elastic Deformations of Compact Stars with Exotic Equations of State, Phys. Rev. Lett. **95**, 211101 (2005).
[80] D. I. Jones, Gravitational wave emission from rotating superfluid neutron stars, Mon. Not. R. Astron. Soc. **402**, 2503 (2010).
[81] D. I. Jones, Parameter choices and ranges for continuous gravitational wave searches for steadily spinning neutron stars, Mon. Not. R. Astron. Soc. **453**, 53 (2015).
[82] D. I. Jones and N. Andersson, Freely precessing neutron stars: Model and observations, Mon. Not. R. Astron. Soc. **324**, 811 (2001).
[83] N. Andersson, D. I. Jones, and W. C. G. Ho, Implications of an r-mode in XTE J1751-305: Mass, radius and spin evolution, Mon. Not. R. Astron. Soc. **442**, 1786 (2014).
[84] A. Idrisy, B. J. Owen, and D. I. Jones, R-mode frequencies of slowly rotating relativistic neutron stars with realistic equations of state, Phys. Rev. D **91**, 024001 (2015).
[85] M. Freitag, P. Amaro-Seoane, and V. Kalogera, Stellar remnants in galactic nuclei: Mass segregation, Astrophys. J. **649**, 91 (2006).
[86] C. J. Hailey, K. Mori, F. E. Bauer, M. E. Berkowitz, J. Hong, and B. J. Hord, A density cusp of quiescent X-ray binaries in

the central parsec of the Galaxy, Nature (London) **556**, 70 (2018).
[87] K. Mori, C. J. Hailey, T. Y. E. Schutt, S. Mandel, K. Heuer, J. E. Grindlay, J. Hong, G. Ponti, and J. A. Tomsick, The x-ray binary population in the Galactic Center revealed through multi-decade observations, Astrophys. J. **921**, 148 (2021).
[88] C. Palomba *et al.*, Direct Constraints on the Ultralight Boson Mass from Searches of Continuous Gravitational Waves, Phys. Rev. Lett. **123**, 171101 (2019).
[89] R. Emami and A. Loeb, Observational signatures of the black hole mass distribution in the Galactic Center, J. Cosmol. Astropart. Phys. 02 (2020) 021.
[90] A. Generozov, N. C. Stone, B. D. Metzger, and J. P. Ostriker, An overabundance of black hole X-ray binaries in the Galactic Centre from tidal captures, Mon. Not. R. Astron. Soc. **478**, 4030 (2018).
[91] G. Ushomirsky, C. Cutler, and L. Bildsten, Deformations of accreting neutron star crusts and gravitational wave emission, Mon. Not. R. Astron. Soc. **319**, 902 (2002).
[92] B. Haskell, D. I. Jones, and N. Andersson, Mountains on neutron stars: Accreted versus non-accreted crusts, Mon. Not. R. Astron. Soc. **373**, 1423 (2006).
[93] R. Bondarescu, S. A. Teukolsky, and I. Wasserman, Spinning down newborn neutron stars: Nonlinear development of the r-mode instability, Phys. Rev. D **79**, 104003 (2009).
[94] P. Jaranowski, A. Królak, and B. F. Schutz, Data analysis of gravitational-wave signals from spinning neutron stars: The signal and its detection, Phys. Rev. D **58**, 063001 (1998).
[95] P. Astone, K. M. Borkowski, P. Jaranowski, and A. Królak, Data analysis of gravitational-wave signals from spinning neutron stars. IV. An all-sky search, Phys. Rev. D **65**, 042003 (2002).

R. Abbott,[1] H. Abe,[2] F. Acernese,[3,4] K. Ackley,[5] N. Adhikari,[6] R. X. Adhikari,[1] V. K. Adkins,[7] V. B. Adya,[8] C. Affeldt,[9,10] D. Agarwal,[11] M. Agathos,[12,13] K. Agatsuma,[14] N. Aggarwal,[15] O. D. Aguiar,[16] L. Aiello,[17] A. Ain,[18] P. Ajith,[19] T. Akutsu,[20,21] S. Albanesi,[22,23] R. A. Alfaidi,[24] A. Allocca,[25,4] P. A. Altin,[8] A. Amato,[26] C. Anand,[5] S. Anand,[1] A. Ananyeva,[1] S. B. Anderson,[1] W. G. Anderson,[6] M. Ando,[27,28] T. Andrade,[29] N. Andres,[30] M. Andrés-Carcasona,[31] T. Andrić,[32] S. V. Angelova,[33] S. Ansoldi,[34,35] J. M. Antelis,[36] S. Antier,[37,38] T. Apostolatos,[39] E. Z. Appavuravther,[40,41] S. Appert,[1] S. K. Apple,[42] K. Arai,[1] A. Araya,[43] M. C. Araya,[1] J. S. Areeda,[44] M. Arène,[45] N. Aritomi,[20] N. Arnaud,[46,47] M. Arogeti,[48] S. M. Aronson,[7] K. G. Arun,[49] H. Asada,[50] Y. Asali,[51] G. Ashton,[52] Y. Aso,[53,54] M. Assiduo,[55,56] S. Assis de Souza Melo,[47] S. M. Aston,[57] P. Astone,[58] F. Aubin,[56] K. AultONeal,[36] C. Austin,[7] S. Babak,[45] F. Badaracco,[59] M. K. M. Bader,[60] C. Badger,[61] S. Bae,[62] Y. Bae,[63] A. M. Baer,[64] S. Bagnasco,[23] Y. Bai,[1] J. Baird,[45] R. Bajpai,[65] T. Baka,[66] M. Ball,[67] G. Ballardin,[47] S. W. Ballmer,[68] A. Balsamo,[64] G. Baltus,[69] S. Banagiri,[15] B. Banerjee,[32] D. Bankar,[11] J. C. Barayoga,[1] C. Barbieri,[70,71,72] B. C. Barish,[1] D. Barker,[73] P. Barneo,[29] F. Barone,[74,4] B. Barr,[24] L. Barsotti,[75] M. Barsuglia,[45] D. Barta,[76] J. Bartlett,[73] M. A. Barton,[24] I. Bartos,[77] S. Basak,[19] R. Bassiri,[78] A. Basti,[79,18] M. Bawaj,[40,80] J. C. Bayley,[24] M. Bazzan,[81,82] B. R. Becher,[83] B. Bécsy,[84] V. M. Bedakihale,[85] F. Beirnaert,[86] M. Bejger,[87] I. Belahcene,[46] V. Benedetto,[88] D. Beniwal,[89] M. G. Benjamin,[90] T. F. Bennett,[91] J. D. Bentley,[14] M. BenYaala,[33] S. Bera,[11] M. Berbel,[92] F. Bergamin,[9,10] B. K. Berger,[78] S. Bernuzzi,[13] D. Bersanetti,[93] A. Bertolini,[60] J. Betzwieser,[57] D. Beveridge,[94] R. Bhandare,[95] A. V. Bhandari,[11] U. Bhardwaj,[38,60] R. Bhatt,[1] D. Bhattacharjee,[96] S. Bhaumik,[77] A. Bianchi,[60,97] I. A. Bilenko,[98] G. Billingsley,[1] S. Bini,[99,100] R. Birney,[101] O. Birnholtz,[102] S. Biscans,[1,75] M. Bischi,[55,56] S. Biscoveanu,[75] A. Bisht,[9,10] B. Biswas,[11] M. Bitossi,[47,18] M.-A. Bizouard,[37] J. K. Blackburn,[1] C. D. Blair,[94] D. G. Blair,[94] R. M. Blair,[73] F. Bobba,[103,104] N. Bode,[9,10] M. Boër,[37] G. Bogaert,[37] M. Boldrini,[105,58] G. N. Bolingbroke,[89] L. D. Bonavena,[81] F. Bondu,[106] E. Bonilla,[78] R. Bonnand,[30] P. Booker,[9,10] B. A. Boom,[60] R. Bork,[1] V. Boschi,[18] N. Bose,[107] S. Bose,[11] V. Bossilkov,[94] V. Boudart,[69] Y. Bouffanais,[81,82] A. Bozzi,[47] C. Bradaschia,[18] P. R. Brady,[6] A. Bramley,[57] A. Branch,[57] M. Branchesi,[32,108] J. E. Brau,[67] M. Breschi,[13] T. Briant,[109] J. H. Briggs,[24] A. Brillet,[37] M. Brinkmann,[9,10] P. Brockill,[6] A. F. Brooks,[1] J. Brooks,[47] D. D. Brown,[89] S. Brunett,[1] G. Bruno,[59] R. Bruntz,[64] J. Bryant,[14] F. Bucci,[56] T. Bulik,[110] H. J. Bulten,[60] A. Buonanno,[111,112] K. Burtnyk,[73] R. Buscicchio,[14] D. Buskulic,[30] C. Buy,[113] R. L. Byer,[78] G. S. Cabourn Davies,[52] G. Cabras,[34,35] R. Cabrita,[59] L. Cadonati,[48] M. Caesar,[114] G. Cagnoli,[26] C. Cahillane,[73] J. Calderón Bustillo,[115] J. D. Callaghan,[24] T. A. Callister,[116,117] E. Calloni,[25,4] J. Cameron,[94] J. B. Camp,[118] M. Canepa,[119,93] S. Canevarolo,[66] M. Cannavacciuolo,[103] K. C. Cannon,[28] H. Cao,[89] Z. Cao,[120] E. Capocasa,[45,20] E. Capote,[68] G. Carapella,[103,104] F. Carbognani,[47] M. Carlassara,[9,10] J. B. Carlin,[121] M. F. Carney,[15] M. Carpinelli,[122,123,47] G. Carrillo,[67] G. Carullo,[79,18] T. L. Carver,[17] J. Casanueva Diaz,[47] C. Casentini,[124,125] G. Castaldi,[126] S. Caudill,[60,66] M. Cavaglià,[96] F. Cavalier,[46] R. Cavalieri,[47] G. Cella,[18] P. Cerdá-Durán,[127] E. Cesarini,[125] W. Chaibi,[37] S. Chalathadka Subrahmanya,[128] E. Champion,[129] C.-H. Chan,[130] C. Chan,[28] C. L. Chan,[131] K. Chan,[131] M. Chan,[132] K. Chandra,[107] I. P. Chang,[130] P. Chanial,[47] S. Chao,[130] C. Chapman-Bird,[24] P. Charlton,[133] E. A. Chase,[15] E. Chassande-Mottin,[45] C. Chatterjee,[94] Debarati Chatterjee,[11]

Deep Chatterjee,[6] M. Chaturvedi,[95] S. Chaty,[45] C. Chen,[134,130] D. Chen,[53] H. Y. Chen,[75] J. Chen,[130] K. Chen,[135] X. Chen,[94] Y.-B. Chen,[136] Y.-R. Chen,[130] Z. Chen,[17] H. Cheng,[77] C. K. Cheong,[131] H. Y. Cheung,[131] H. Y. Chia,[77] F. Chiadini,[137,104] C-Y. Chiang,[138] G. Chiarini,[82] R. Chierici,[139] A. Chincarini,[93] M. L. Chiofalo,[79,18] A. Chiummo,[47] R. K. Choudhary,[94] S. Choudhary,[11] N. Christensen,[37] Q. Chu,[94] Y-K. Chu,[138] S. S. Y. Chua,[8] K. W. Chung,[61] G. Ciani,[81,82] P. Ciecielag,[87] M. Cieślar,[87] M. Cifaldi,[124,125] A. A. Ciobanu,[89] R. Ciolfi,[140,82] F. Cipriano,[37] F. Clara,[73] J. A. Clark,[1,48] P. Clearwater,[141] S. Clesse,[142] F. Cleva,[37] E. Coccia,[32,108] E. Codazzo,[32] P.-F. Cohadon,[109] D. E. Cohen,[46] M. Colleoni,[143] C. G. Collette,[144] A. Colombo,[70,71] M. Colpi,[70,71] C. M. Compton,[73] M. Constancio Jr.,[16] L. Conti,[82] S. J. Cooper,[14] P. Corban,[57] T. R. Corbitt,[7] I. Cordero-Carrión,[145] S. Corezzi,[80,40] K. R. Corley,[51] N. J. Cornish,[84] D. Corre,[46] A. Corsi,[146] S. Cortese,[47] C. A. Costa,[16] R. Cotesta,[112] R. Cottingham,[57] M. W. Coughlin,[147] J.-P. Coulon,[37] S. T. Countryman,[51] B. Cousins,[148] P. Couvares,[1] D. M. Coward,[94] M. J. Cowart,[57] D. C. Coyne,[1] R. Coyne,[149] J. D. E. Creighton,[6] T. D. Creighton,[90] A. W. Criswell,[147] M. Croquette,[109] S. G. Crowder,[150] J. R. Cudell,[69] T. J. Cullen,[7] A. Cumming,[24] R. Cummings,[24] L. Cunningham,[24] E. Cuoco,[47,151,18] M. Curyło,[110] P. Dabadie,[26] T. Dal Canton,[46] S. Dall'Osso,[32] G. Dálya,[86,152] A. Dana,[78] B. D'Angelo,[119,93] S. Danilishin,[153,60] S. D'Antonio,[125] K. Danzmann,[9,10] C. Darsow-Fromm,[128] A. Dasgupta,[85] L. E. H. Datrier,[24] Sayak Datta,[11] Sayantani Datta,[49] V. Dattilo,[47] I. Dave,[95] M. Davier,[46] D. Davis,[1] M. C. Davis,[114] E. J. Daw,[154] R. Dean,[114] D. DeBra,[78] M. Deenadayalan,[11] J. Degallaix,[155] M. De Laurentis,[25,4] S. Deléglise,[109] V. Del Favero,[129] F. De Lillo,[59] N. De Lillo,[24] D. Dell'Aquila,[122] W. Del Pozzo,[79,18] L. M. DeMarchi,[15] F. De Matteis,[124,125] V. D'Emilio,[17] N. Demos,[75] T. Dent,[115] A. Depasse,[59] R. De Pietri,[156,157] R. De Rosa,[25,4] C. De Rossi,[47] R. DeSalvo,[126,158] R. De Simone,[137] S. Dhurandhar,[11] M. C. Díaz,[90] N. A. Didio,[68] T. Dietrich,[112] L. Di Fiore,[4] C. Di Fronzo,[14] C. Di Giorgio,[103,104] F. Di Giovanni,[127] M. Di Giovanni,[32] T. Di Girolamo,[25,4] A. Di Lieto,[79,18] A. Di Michele,[80] B. Ding,[144] S. Di Pace,[105,58] I. Di Palma,[105,58] F. Di Renzo,[79,18] A. K. Divakarla,[77] A. Dmitriev,[14] Z. Doctor,[15] L. Donahue,[159] L. D'Onofrio,[25,4] F. Donovan,[75] K. L. Dooley,[17] S. Doravari,[11] M. Drago,[105,58] J. C. Driggers,[73] Y. Drori,[1] J.-G. Ducoin,[46] P. Dupej,[24] U. Dupletsa,[32] O. Durante,[103,104] D. D'Urso,[122,123] P.-A. Duverne,[46] S. E. Dwyer,[73] C. Eassa,[73] P. J. Easter,[5] M. Ebersold,[160] T. Eckhardt,[128] G. Eddolls,[24] B. Edelman,[67] T. B. Edo,[1] O. Edy,[52] A. Effler,[57] S. Eguchi,[132] J. Eichholz,[8] S. S. Eikenberry,[77] M. Eisenmann,[30,20] R. A. Eisenstein,[75] A. Ejlli,[17] E. Engelby,[44] Y. Enomoto,[27] L. Errico,[25,4] R. C. Essick,[161] H. Estellés,[143] D. Estevez,[162] Z. Etienne,[163] T. Etzel,[1] M. Evans,[75] T. M. Evans,[57] T. Evstafyeva,[12] B. E. Ewing,[148] F. Fabrizi,[55,56] F. Faedi,[56] V. Fafone,[124,125,32] H. Fair,[68] S. Fairhurst,[17] P. C. Fan,[159] A. M. Farah,[164] S. Farinon,[93] B. Farr,[67] W. M. Farr,[116,117] E. J. Fauchon-Jones,[17] G. Favaro,[81] M. Favata,[165] M. Fays,[69] M. Fazio,[166] J. Feicht,[1] M. M. Fejer,[78] E. Fenyvesi,[76,167] D. L. Ferguson,[168] A. Fernandez-Galiana,[75] I. Ferrante,[79,18] T. A. Ferreira,[16] F. Fidecaro,[79,18] P. Figura,[110] A. Fiori,[18,79] I. Fiori,[47] M. Fishbach,[15] R. P. Fisher,[64] R. Fittipaldi,[169,104] V. Fiumara,[170,104] R. Flaminio,[30,20] E. Floden,[147] H. K. Fong,[28] J. A. Font,[127,171] B. Fornal,[158] P. W. F. Forsyth,[8] A. Franke,[128] S. Frasca,[105,58] F. Frasconi,[18] J. P. Freed,[36] Z. Frei,[152] A. Freise,[60,97] O. Freitas,[172] R. Frey,[67] P. Fritschel,[75] V. V. Frolov,[57] G. G. Fronzé,[23] Y. Fujii,[173] Y. Fujikawa,[174] Y. Fujimoto,[175] P. Fulda,[77] M. Fyffe,[57] H. A. Gabbard,[24] W. E. Gabella,[176] B. U. Gadre,[112] J. R. Gair,[112] J. Gais,[131] S. Galaudage,[5] R. Gamba,[13] D. Ganapathy,[75] A. Ganguly,[11] D. Gao,[177] S. G. Gaonkar,[11] B. Garaventa,[93,119] C. García Núñez,[101] C. García-Quirós,[143] F. Garufi,[25,4] B. Gateley,[73] V. Gayathri,[77] G.-G. Ge,[177] G. Gemme,[93] A. Gennai,[18] J. George,[95] O. Gerberding,[128] L. Gergely,[178] P. Gewecke,[128] S. Ghonge,[48] Abhirup Ghosh,[112] Archisman Ghosh,[86] Shaon Ghosh,[165] Shrobana Ghosh,[17] Tathagata Ghosh,[11] B. Giacomazzo,[70,71,72] L. Giacoppo,[105,58] J. A. Giaime,[7,57] K. D. Giardina,[57] D. R. Gibson,[101] C. Gier,[33] M. Giesler,[179] P. Giri,[18,79] F. Gissi,[88] S. Gkaitatzis,[18,79] J. Glanzer,[7] A. E. Gleckl,[44] P. Godwin,[148] E. Goetz,[180] R. Goetz,[77] N. Gohlke,[9,10] J. Golomb,[1] B. Goncharov,[32] G. González,[7] M. Gosselin,[47] R. Gouaty,[30] D. W. Gould,[8] S. Goyal,[19] B. Grace,[8] A. Grado,[181,4] V. Graham,[24] M. Granata,[155] V. Granata,[103] A. Grant,[24] S. Gras,[75] P. Grassia,[1] C. Gray,[73] R. Gray,[24] G. Greco,[40] A. C. Green,[77] R. Green,[17] A. M. Gretarsson,[36] E. M. Gretarsson,[36] D. Griffith,[1] W. L. Griffiths,[17] H. L. Griggs,[48] G. Grignani,[80,40] A. Grimaldi,[99,100] E. Grimes,[36] S. J. Grimm,[32,108] H. Grote,[17] S. Grunewald,[112] P. Gruning,[46] A. S. Gruson,[44] D. Guerra,[127] G. M. Guidi,[55,56] A. R. Guimaraes,[7] G. Guixé,[29] H. K. Gulati,[85] A. M. Gunny,[75] H.-K. Guo,[158] Y. Guo,[60] Anchal Gupta,[1] Anuradha Gupta,[182] I. M. Gupta,[148] P. Gupta,[60,66] S. K. Gupta,[107] R. Gustafson,[183] F. Guzman,[184] S. Ha,[185] I. P. W. Hadiputrawan,[135] L. Haegel,[45] S. Haino,[138] O. Halim,[35] E. D. Hall,[75] E. Z. Hamilton,[160] G. Hammond,[24] W.-B. Han,[186] M. Haney,[160] J. Hanks,[73] C. Hanna,[148] M. D. Hannam,[17] O. Hannuksela,[66,60] H. Hansen,[73] T. J. Hansen,[36] J. Hanson,[57] T. Harder,[37] K. Haris,[60,66] J. Harms,[32,108] G. M. Harry,[42] I. W. Harry,[52] D. Hartwig,[128] K. Hasegawa,[187] B. Haskell,[87] C.-J. Haster,[75] J. S. Hathaway,[129] K. Hattori,[188] K. Haughian,[24] H. Hayakawa,[189] K. Hayama,[132] F. J. Hayes,[24] J. Healy,[129] A. Heidmann,[109] A. Heidt,[9,10] M. C. Heintze,[57] J. Heinze,[9,10] J. Heinzel,[75] H. Heitmann,[37] F. Hellman,[190] P. Hello,[46] A. F. Helmling-Cornell,[67]

G. Hemming,[47] M. Hendry,[24] I. S. Heng,[24] E. Hennes,[60] J. Hennig,[191] M. H. Hennig,[191] C. Henshaw,[48] A. G. Hernandez,[91] F. Hernandez Vivanco,[5] M. Heurs,[9,10] A. L. Hewitt,[192] S. Higginbotham,[17] S. Hild,[153,60] P. Hill,[33] Y. Himemoto,[193] A. S. Hines,[184] N. Hirata,[20] C. Hirose,[174] T-C. Ho,[135] S. Hochheim,[9,10] D. Hofman,[155] J. N. Hohmann,[128] D. G. Holcomb,[114] N. A. Holland,[8] I. J. Hollows,[154] Z. J. Holmes,[89] K. Holt,[57] D. E. Holz,[164] Q. Hong,[130] J. Hough,[24] S. Hourihane,[1] E. J. Howell,[94] C. G. Hoy,[17] D. Hoyland,[14] A. Hreibi,[9,10] B-H. Hsieh,[187] H-F. Hsieh,[130] C. Hsiung,[134] Y. Hsu,[130] H-Y. Huang,[138] P. Huang,[177] Y-C. Huang,[130] Y.-J. Huang,[138] Yiting Huang,[150] Yiwen Huang,[75] M. T. Hübner,[5] A. D. Huddart,[194] B. Hughey,[36] D. C. Y. Hui,[195] V. Hui,[30] S. Husa,[143] S. H. Huttner,[24] R. Huxford,[148] T. Huynh-Dinh,[57] S. Ide,[196] B. Idzkowski,[110] A. Iess,[124,125] K. Inayoshi,[197] Y. Inoue,[135] P. Iosif,[198] M. Isi,[75] K. Isleif,[128] K. Ito,[199] Y. Itoh,[175,200] B. R. Iyer,[19] V. JaberianHamedan,[94] T. Jacqmin,[109] P.-E. Jacquet,[109] S. J. Jadhav,[201] S. P. Jadhav,[11] T. Jain,[12] A. L. James,[17] A. Z. Jan,[168] K. Jani,[176] J. Janquart,[66,60] K. Janssens,[202,37] N. N. Janthalur,[201] P. Jaranowski,[203] D. Jariwala,[77] R. Jaume,[143] A. C. Jenkins,[61] K. Jenner,[89] C. Jeon,[204] W. Jia,[75] J. Jiang,[77] H.-B. Jin,[205,206] G. R. Johns,[64] R. Johnston,[24] A. W. Jones,[94] D. I. Jones,[207] P. Jones,[14] R. Jones,[24] P. Joshi,[148] L. Ju,[94] A. Jue,[158] P. Jung,[63] K. Jung,[185] J. Junker,[9,10] V. Juste,[162] K. Kaihotsu,[199] T. Kajita,[208] M. Kakizaki,[188] C. V. Kalaghatgi,[17,66,60,209] V. Kalogera,[15] B. Kamai,[1] M. Kamiizumi,[189] N. Kanda,[175,200] S. Kandhasamy,[11] G. Kang,[210] J. B. Kanner,[1] Y. Kao,[130] S. J. Kapadia,[19] D. P. Kapasi,[8] C. Karathanasis,[31] S. Karki,[96] R. Kashyap,[148] M. Kasprzack,[1] W. Kastaun,[9,10] T. Kato,[187] S. Katsanevas,[47] E. Katsavounidis,[75] W. Katzman,[57] T. Kaur,[94] K. Kawabe,[73] K. Kawaguchi,[187] F. Kéfélian,[37] D. Keitel,[143] J. S. Key,[211] S. Khadka,[78] F. Y. Khalili,[98] S. Khan,[17] T. Khanam,[146] E. A. Khazanov,[212] N. Khetan,[32,108] M. Khursheed,[95] N. Kijbunchoo,[8] A. Kim,[15] C. Kim,[204] J. C. Kim,[213] J. Kim,[214] K. Kim,[204] W. S. Kim,[63] Y.-M. Kim,[185] C. Kimball,[15] N. Kimura,[189] M. Kinley-Hanlon,[24] R. Kirchhoff,[9,10] J. S. Kissel,[73] S. Klimenko,[77] T. Klinger,[12] A. M. Knee,[180] T. D. Knowles,[163] N. Knust,[9,10] E. Knyazev,[75] Y. Kobayashi,[175] P. Koch,[9,10] G. Koekoek,[60,153] K. Kohri,[215] K. Kokeyama,[216] S. Koley,[32] P. Kolitsidou,[17] M. Kolstein,[31] K. Komori,[75] V. Kondrashov,[1] A. K. H. Kong,[130] A. Kontos,[83] N. Koper,[9,10] M. Korobko,[128] M. Kovalam,[94] N. Koyama,[174] D. B. Kozak,[1] C. Kozakai,[53] V. Kringel,[9,10] N. V. Krishnendu,[9,10] A. Królak,[217,218] G. Kuehn,[9,10] F. Kuei,[130] P. Kuijer,[60] S. Kulkarni,[182] A. Kumar,[201] Prayush Kumar,[19] Rahul Kumar,[73] Rakesh Kumar,[85] J. Kume,[28] K. Kuns,[75] Y. Kuromiya,[199] S. Kuroyanagi,[219,220] K. Kwak,[185] G. Lacaille,[24] P. Lagabbe,[30] D. Laghi,[113] E. Lalande,[221] M. Lalleman,[202] T. L. Lam,[131] A. Lamberts,[37,222] M. Landry,[73] B. B. Lane,[75] R. N. Lang,[75] J. Lange,[168] B. Lantz,[78] I. La Rosa,[30] A. Lartaux-Vollard,[46] P. D. Lasky,[5] M. Laxen,[57] A. Lazzarini,[1] C. Lazzaro,[81,82] P. Leaci,[105,58] S. Leavey,[9,10] S. LeBohec,[158] Y. K. Lecoeuche,[180] E. Lee,[187] H. M. Lee,[223] H. W. Lee,[213] K. Lee,[224] R. Lee,[130] I. N. Legred,[1] J. Lehmann,[9,10] A. Lemaître,[225] M. Lenti,[56,226] M. Leonardi,[20] E. Leonova,[38] N. Leroy,[46] N. Letendre,[30] C. Levesque,[221] Y. Levin,[5] J. N. Leviton,[183] K. Leyde,[45] A. K. Y. Li,[1] B. Li,[130] J. Li,[15] K. L. Li,[227] P. Li,[228] T. G. F. Li,[131] X. Li,[136] C-Y. Lin,[229] E. T. Lin,[130] F-K. Lin,[138] F-L. Lin,[230] H. L. Lin,[135] L. C.-C. Lin,[227] F. Linde,[209,60] S. D. Linker,[126,91] J. N. Linley,[24] T. B. Littenberg,[231] G. C. Liu,[134] J. Liu,[94] K. Liu,[130] X. Liu,[6] F. Llamas,[90] R. K. L. Lo,[1] T. Lo,[130] L. T. London,[38,75] A. Longo,[232] D. Lopez,[160] M. Lopez Portilla,[66] M. Lorenzini,[124,125] V. Loriette,[233] M. Lormand,[57] G. Losurdo,[18] T. P. Lott,[48] J. D. Lough,[9,10] C. O. Lousto,[129] G. Lovelace,[44] J. F. Lucaccioni,[234] H. Lück,[9,10] D. Lumaca,[124,125] A. P. Lundgren,[52] L.-W. Luo,[138] J. E. Lynam,[64] M. Ma'arif,[135] R. Macas,[52] J. B. Machtinger,[15] M. MacInnis,[75] D. M. Macleod,[17] I. A. O. MacMillan,[1] A. Macquet,[37] I. Magaña Hernandez,[6] C. Magazzù,[18] R. M. Magee,[1] R. Maggiore,[14] M. Magnozzi,[93,119] S. Mahesh,[163] E. Majorana,[105,58] I. Maksimovic,[233] S. Maliakal,[1] A. Malik,[95] N. Man,[37] V. Mandic,[147] V. Mangano,[105,58] G. L. Mansell,[73,75] M. Manske,[6] M. Mantovani,[47] M. Mapelli,[81,82] F. Marchesoni,[41,40,235] D. Marín Pina,[29] F. Marion,[30] Z. Mark,[136] S. Márka,[51] Z. Márka,[51] C. Markakis,[12] A. S. Markosyan,[78] A. Markowitz,[1] E. Maros,[1] A. Marquina,[145] S. Marsat,[45] F. Martelli,[55,56] I. W. Martin,[24] R. M. Martin,[165] M. Martinez,[31] V. A. Martinez,[77] V. Martinez,[26] K. Martinovic,[61] D. V. Martynov,[14] E. J. Marx,[75] H. Masalehdan,[128] K. Mason,[75] E. Massera,[154] A. Masserot,[30] M. Masso-Reid,[24] S. Mastrogiovanni,[45] A. Matas,[112] M. Mateu-Lucena,[143] F. Matichard,[1,75] M. Matiushechkina,[9,10] N. Mavalvala,[75] J. J. McCann,[94] R. McCarthy,[73] D. E. McClelland,[8] P. K. McClincy,[148] S. McCormick,[57] L. McCuller,[75] G. I. McGhee,[24] S. C. McGuire,[57] C. McIsaac,[52] J. McIver,[180] T. McRae,[8] S. T. McWilliams,[163] D. Meacher,[6] M. Mehmet,[9,10] A. K. Mehta,[112] Q. Meijer,[66] A. Melatos,[121] D. A. Melchor,[44] G. Mendell,[73] A. Menendez-Vazquez,[31] C. S. Menoni,[166] R. A. Mercer,[6] L. Mereni,[155] K. Merfeld,[67] E. L. Merilh,[57] J. D. Merritt,[67] M. Merzougui,[37] S. Meshkov,[1,†] C. Messenger,[24] C. Messick,[75] P. M. Meyers,[121] F. Meylahn,[9,10] A. Mhaske,[11] A. Miani,[99,100] H. Miao,[14] I. Michaloliakos,[77] C. Michel,[155] Y. Michimura,[27] H. Middleton,[121] D. P. Mihaylov,[112] L. Milano,[25,†] A. L. Miller,[59] A. Miller,[91] B. Miller,[38,60] M. Millhouse,[121] J. C. Mills,[17] E. Milotti,[236,35] Y. Minenkov,[125] N. Mio,[237] Ll. M. Mir,[31] M. Miravet-Tenés,[127] A. Mishkin,[77] C. Mishra,[238] T. Mishra,[77] T. Mistry,[154] S. Mitra,[11] V. P. Mitrofanov,[98] G. Mitselmakher,[77] R. Mittleman,[75] O. Miyakawa,[189] K. Miyo,[189] S. Miyoki,[189]

Geoffrey Mo,[75] L. M. Modafferi,[143] E. Moguel,[234] K. Mogushi,[96] S. R. P. Mohapatra,[75] S. R. Mohite,[6] I. Molina,[44] M. Molina-Ruiz,[190] M. Mondin,[91] M. Montani,[55,56] C. J. Moore,[14] J. Moragues,[143] D. Moraru,[73] F. Morawski,[87] A. More,[11] C. Moreno,[36] G. Moreno,[73] Y. Mori,[199] S. Morisaki,[6] N. Morisue,[175] Y. Moriwaki,[188] B. Mours,[162] C. M. Mow-Lowry,[60,97] S. Mozzon,[52] F. Muciaccia,[105,58] Arunava Mukherjee,[239] D. Mukherjee,[148] Soma Mukherjee,[90] Subroto Mukherjee,[85] Suvodip Mukherjee,[161,38] N. Mukund,[9,10] A. Mullavey,[57] J. Munch,[89] E. A. Muñiz,[68] P. G. Murray,[24] R. Musenich,[93,119] S. Muusse,[89] S. L. Nadji,[9,10] K. Nagano,[240] A. Nagar,[23,241] K. Nakamura,[20] H. Nakano,[242] M. Nakano,[187] Y. Nakayama,[199] V. Napolano,[47] I. Nardecchia,[124,125] T. Narikawa,[187] H. Narola,[66] L. Naticchioni,[58] B. Nayak,[91] R. K. Nayak,[243] B. F. Neil,[94] J. Neilson,[88,104] A. Nelson,[184] T. J. N. Nelson,[57] M. Nery,[9,10] P. Neubauer,[234] A. Neunzert,[211] K. Y. Ng,[75] S. W. S. Ng,[89] C. Nguyen,[45] P. Nguyen,[67] T. Nguyen,[75] L. Nguyen Quynh,[244] J. Ni,[147] W.-T. Ni,[205,177,130] S. A. Nichols,[7] T. Nishimoto,[187] A. Nishizawa,[28] S. Nissanke,[38,60] E. Nitoglia,[139] F. Nocera,[47] M. Norman,[17] C. North,[17] S. Nozaki,[188] G. Nurbek,[90] L. K. Nuttall,[52] Y. Obayashi,[187] J. Oberling,[73] B. D. O'Brien,[77] J. O'Dell,[194] E. Oelker,[24] W. Ogaki,[187] G. Oganesyan,[32,108] J. J. Oh,[63] K. Oh,[195] S. H. Oh,[63] M. Ohashi,[189] T. Ohashi,[175] M. Ohkawa,[174] F. Ohme,[9,10] H. Ohta,[28] M. A. Okada,[16] Y. Okutani,[196] C. Olivetto,[47] K. Oohara,[187,245] R. Oram,[57] B. O'Reilly,[57] R. G. Ormiston,[147] N. D. Ormsby,[64] R. O'Shaughnessy,[129] E. O'Shea,[179] S. Oshino,[189] S. Ossokine,[112] C. Osthelder,[1] S. Otabe,[2] D. J. Ottaway,[89] H. Overmier,[57] A. E. Pace,[148] G. Pagano,[79,18] R. Pagano,[7] M. A. Page,[94] G. Pagliaroli,[32,108] A. Pai,[107] S. A. Pai,[95] S. Pal,[243] J. R. Palamos,[67] O. Palashov,[212] C. Palomba,[58] H. Pan,[130] K.-C. Pan,[130] P. K. Panda,[201] P. T. H. Pang,[60,66] C. Pankow,[15] F. Pannarale,[105,58] B. C. Pant,[95] F. H. Panther,[94] F. Paoletti,[18] A. Paoli,[47] A. Paolone,[58,246] G. Pappas,[198] A. Parisi,[134] H. Park,[6] J. Park,[247] W. Parker,[57] D. Pascucci,[60,86] A. Pasqualetti,[47] R. Passaquieti,[79,18] D. Passuello,[18] M. Patel,[64] M. Pathak,[89] B. Patricelli,[47,18] A. S. Patron,[7] S. Paul,[67] E. Payne,[5] M. Pedraza,[1] R. Pedurand,[104] M. Pegoraro,[82] A. Pele,[57] F. E. Peña Arellano,[189] S. Penano,[78] S. Penn,[248] A. Perego,[99,100] A. Pereira,[26] T. Pereira,[249] C. J. Perez,[73] C. Périgois,[30] C. C. Perkins,[77] A. Perreca,[99,100] S. Perriès,[139] D. Pesios,[198] J. Petermann,[128] D. Petterson,[1] H. P. Pfeiffer,[112] H. Pham,[57] K. A. Pham,[147] K. S. Phukon,[60,209] H. Phurailatpam,[131] O. J. Piccinni,[58] M. Pichot,[37] M. Piendibene,[79,18] F. Piergiovanni,[55,56] L. Pierini,[105,58] V. Pierro,[88,104] G. Pillant,[47] M. Pillas,[46] F. Pilo,[18] L. Pinard,[155] C. Pineda-Bosque,[91] I. M. Pinto,[88,104,250] M. Pinto,[47] B. J. Piotrzkowski,[6] K. Piotrzkowski,[59] M. Pirello,[73] M. D. Pitkin,[192] A. Placidi,[40,80] E. Placidi,[105,58] M. L. Planas,[143] W. Plastino,[251,232] C. Pluchar,[252] R. Poggiani,[79,18] E. Polini,[30] D. Y. T. Pong,[131] S. Ponrathnam,[11] E. K. Porter,[45] R. Poulton,[47] A. Poverman,[83] J. Powell,[141] M. Pracchia,[30] T. Pradier,[162] A. K. Prajapati,[85] K. Prasai,[78] R. Prasanna,[201] G. Pratten,[14] M. Principe,[88,250,104] G. A. Prodi,[253,100] L. Prokhorov,[14] P. Prosposito,[124,125] L. Prudenzi,[112] A. Puecher,[60,66] M. Punturo,[40] F. Puosi,[18,79] P. Puppo,[58] M. Pürrer,[112] H. Qi,[17] N. Quartey,[64] V. Quetschke,[90] P. J. Quinonez,[36] R. Quitzow-James,[96] F. J. Raab,[73] G. Raaijmakers,[38,60] H. Radkins,[73] N. Radulesco,[37] P. Raffai,[152] S. X. Rail,[221] S. Raja,[95] C. Rajan,[95] K. E. Ramirez,[57] T. D. Ramirez,[44] A. Ramos-Buades,[112] J. Rana,[148] P. Rapagnani,[105,58] A. Ray,[6] V. Raymond,[17] N. Raza,[180] M. Razzano,[79,18] J. Read,[44] L. A. Rees,[42] T. Regimbau,[30] L. Rei,[93] S. Reid,[33] S. W. Reid,[64] D. H. Reitze,[1,77] P. Relton,[17] A. Renzini,[1] P. Rettegno,[22,23] B. Revenu,[45] A. Reza,[60] M. Rezac,[44] F. Ricci,[105,58] D. Richards,[194] J. W. Richardson,[254] L. Richardson,[184] G. Riemenschneider,[22,23] K. Riles,[183] S. Rinaldi,[79,18] K. Rink,[180] N. A. Robertson,[1] R. Robie,[1] F. Robinet,[46] A. Rocchi,[125] S. Rodriguez,[44] L. Rolland,[30] J. G. Rollins,[1] M. Romanelli,[106] R. Romano,[3,4] C. L. Romel,[73] A. Romero,[31] I. M. Romero-Shaw,[5] J. H. Romie,[57] S. Ronchini,[32,108] L. Rosa,[4,25] C. A. Rose,[6] D. Rosińska,[110] M. P. Ross,[255] S. Rowan,[24] S. J. Rowlinson,[14] Santosh Roy,[11] Soumen Roy,[256,66] D. Rozza,[122,123] P. Ruggi,[47] K. Ruiz-Rocha,[176] K. Ryan,[73] S. Sachdev,[148] T. Sadecki,[73] J. Sadiq,[115] S. Saha,[130] Y. Saito,[189] K. Sakai,[257] M. Sakellariadou,[61] S. Sakon,[148] O. S. Salafia,[72,71,70] F. Salces-Carcoba,[1] L. Salconi,[47] M. Saleem,[147] F. Salemi,[99,100] A. Samajdar,[71] E. J. Sanchez,[1] J. H. Sanchez,[44] L. E. Sanchez,[1] N. Sanchis-Gual,[258] J. R. Sanders,[259] A. Sanuy,[29] T. R. Saravanan,[11] N. Sarin,[5] B. Sassolas,[155] H. Satari,[94] O. Sauter,[77] R. L. Savage,[73] V. Savant,[11] T. Sawada,[175] H. L. Sawant,[11] S. Sayah,[155] D. Schaetzl,[1] M. Scheel,[136] J. Scheuer,[15] M. G. Schiworski,[89] P. Schmidt,[14] S. Schmidt,[66] R. Schnabel,[128] M. Schneewind,[9,10] R. M. S. Schofield,[67] A. Schönbeck,[128] B. W. Schulte,[9,10] B. F. Schutz,[17,9,10] E. Schwartz,[17] J. Scott,[24] S. M. Scott,[8] M. Seglar-Arroyo,[30] Y. Sekiguchi,[260] D. Sellers,[57] A. S. Sengupta,[256] D. Sentenac,[47] E. G. Seo,[131] V. Sequino,[25,4] A. Sergeev,[212] Y. Setyawati,[9,10,66] T. Shaffer,[73] M. S. Shahriar,[15] M. A. Shaikh,[19] B. Shams,[158] L. Shao,[197] A. Sharma,[32,108] P. Sharma,[95] P. Shawhan,[111] N. S. Shcheblanov,[225] A. Sheela,[238] Y. Shikano,[261,262] M. Shikauchi,[28] H. Shimizu,[263] K. Shimode,[189] H. Shinkai,[264] T. Shishido,[54] A. Shoda,[20] D. H. Shoemaker,[75] D. M. Shoemaker,[168] S. ShyamSundar,[95] M. Sieniawska,[59] D. Sigg,[73] L. Silenzi,[40,41] L. P. Singer,[118] D. Singh,[148] M. K. Singh,[19] N. Singh,[110] A. Singha,[153,60] A. M. Sintes,[143] V. Sipala,[122,123] V. Skliris,[17] B. J. J. Slagmolen,[8] T. J. Slaven-Blair,[94] J. Smetana,[14] J. R. Smith,[44] L. Smith,[24] R. J. E. Smith,[5] J. Soldateschi,[226,265,56] S. N. Somala,[266] K. Somiya,[2] I. Song,[130] K. Soni,[11] S. Soni,[75] V. Sordini,[139]

F. Sorrentino,[93] N. Sorrentino,[79,18] R. Soulard,[37] T. Souradeep,[267,11] E. Sowell,[146] V. Spagnuolo,[153,60] A. P. Spencer,[24] M. Spera,[81,82] P. Spinicelli,[47] A. K. Srivastava,[85] V. Srivastava,[68] K. Staats,[15] C. Stachie,[37] F. Stachurski,[24] D. A. Steer,[45] J. Steinlechner,[153,60] S. Steinlechner,[153,60] N. Stergioulas,[198] D. J. Stops,[14] M. Stover,[234] K. A. Strain,[24] L. C. Strang,[121] G. Stratta,[268,58] M. D. Strong,[7] A. Strunk,[73] R. Sturani,[249] A. L. Stuver,[114] M. Suchenek,[87] S. Sudhagar,[11] V. Sudhir,[75] R. Sugimoto,[269,240] H. G. Suh,[6] A. G. Sullivan,[51] T. Z. Summerscales,[270] L. Sun,[8] S. Sunil,[85] A. Sur,[87] J. Suresh,[28] P. J. Sutton,[17] Takamasa Suzuki,[174] Takanori Suzuki,[2] Toshikazu Suzuki,[187] B. L. Swinkels,[60] M. J. Szczepańczyk,[77] P. Szewczyk,[110] M. Tacca,[60] H. Tagoshi,[187] S. C. Tait,[24] H. Takahashi,[271] R. Takahashi,[20] S. Takano,[27] H. Takeda,[27] M. Takeda,[175] C. J. Talbot,[33] C. Talbot,[1] K. Tanaka,[272] Taiki Tanaka,[187] Takahiro Tanaka,[273] A. J. Tanasijczuk,[59] S. Tanioka,[189] D. B. Tanner,[77] D. Tao,[1] L. Tao,[77] R. D. Tapia,[148] E. N. Tapia San Martín,[60] C. Taranto,[124] A. Taruya,[274] J. D. Tasson,[159] R. Tenorio,[143] J. E. S. Terhune,[114] L. Terkowski,[128] M. P. Thirugnanasambandam,[11] M. Thomas,[57] P. Thomas,[73] E. E. Thompson,[48] J. E. Thompson,[17] S. R. Thondapu,[95] K. A. Thorne,[57] E. Thrane,[5] Shubhanshu Tiwari,[160] Srishti Tiwari,[11] V. Tiwari,[17] A. M. Toivonen,[147] A. E. Tolley,[52] T. Tomaru,[20] T. Tomura,[189] M. Tonelli,[79,18] Z. Tornasi,[24] A. Torres-Forné,[127] C. I. Torrie,[1] I. Tosta e Melo,[123] D. Töyrä,[8] A. Trapananti,[41,40] F. Travasso,[40,41] G. Traylor,[57] M. Trevor,[111] M. C. Tringali,[47] A. Tripathee,[183] L. Troiano,[275,104] A. Trovato,[45] L. Trozzo,[4,189] R. J. Trudeau,[1] D. Tsai,[130] K. W. Tsang,[60,276,66] T. Tsang,[277] J-S. Tsao,[230] M. Tse,[75] R. Tso,[136] S. Tsuchida,[175] L. Tsukada,[148] D. Tsuna,[28] T. Tsutsui,[28] K. Turbang,[278,202] M. Turconi,[37] D. Tuyenbayev,[175] A. S. Ubhi,[14] N. Uchikata,[187] T. Uchiyama,[189] R. P. Udall,[1] A. Ueda,[279] T. Uehara,[280,281] K. Ueno,[28] G. Ueshima,[282] C. S. Unnikrishnan,[283] A. L. Urban,[7] T. Ushiba,[189] A. Utina,[153,60] G. Vajente,[1] A. Vajpeyi,[5] G. Valdes,[184] M. Valentini,[182,99,100] V. Valsan,[6] N. van Bakel,[60] M. van Beuzekom,[60] M. van Dael,[60,284] J. F. J. van den Brand,[153,97,60] C. Van Den Broeck,[66,60] D. C. Vander-Hyde,[68] H. van Haevermaet,[202] J. V. van Heijningen,[59] M. H. P. M. van Putten,[285] N. van Remortel,[202] M. Vardaro,[209,60] A. F. Vargas,[121] V. Varma,[112] M. Vasúth,[76] A. Vecchio,[14] G. Vedovato,[82] J. Veitch,[24] P. J. Veitch,[89] J. Venneberg,[9,10] G. Venugopalan,[1] D. Verkindt,[30] P. Verma,[218] Y. Verma,[95] S. M. Vermeulen,[17] D. Veske,[51] F. Vetrano,[55] A. Viceré,[55,56] S. Vidyant,[68] A. D. Viets,[286] A. Vijaykumar,[19] V. Villa-Ortega,[115] J.-Y. Vinet,[37] A. Virtuoso,[236,35] S. Vitale,[75] H. Vocca,[80,40] E. R. G. von Reis,[73] J. S. A. von Wrangel,[9,10] C. Vorvick,[73] S. P. Vyatchanin,[98] L. E. Wade,[234] M. Wade,[234] K. J. Wagner,[129] R. C. Walet,[60] M. Walker,[64] G. S. Wallace,[33] L. Wallace,[1] J. Wang,[177] J. Z. Wang,[183] W. H. Wang,[90] R. L. Ward,[8] J. Warner,[73] M. Was,[30] T. Washimi,[20] N. Y. Washington,[1] J. Watchi,[144] B. Weaver,[73] C. R. Weaving,[52] S. A. Webster,[24] M. Weinert,[9,10] A. J. Weinstein,[1] R. Weiss,[75] C. M. Weller,[255] R. A. Weller,[176] F. Wellmann,[9,10] L. Wen,[94] P. Weßels,[9,10] K. Wette,[8] J. T. Whelan,[129] D. D. White,[44] B. F. Whiting,[77] C. Whittle,[75] D. Wilken,[9,10] D. Williams,[24] M. J. Williams,[24] A. R. Williamson,[52] J. L. Willis,[1] B. Willke,[9,10] D. J. Wilson,[252] C. C. Wipf,[1] T. Wlodarczyk,[112] G. Woan,[24] J. Woehler,[9,10] J. K. Wofford,[129] D. Wong,[180] I. C. F. Wong,[131] M. Wright,[24] C. Wu,[130] D. S. Wu,[9,10] H. Wu,[130] D. M. Wysocki,[6] L. Xiao,[1] T. Yamada,[263] H. Yamamoto,[1] K. Yamamoto,[188] T. Yamamoto,[189] K. Yamashita,[199] R. Yamazaki,[196] F. W. Yang,[158] K. Z. Yang,[147] L. Yang,[166] Y.-C. Yang,[130] Y. Yang,[287] Yang Yang,[77] M. J. Yap,[8] D. W. Yeeles,[17] S.-W. Yeh,[130] A. B. Yelikar,[129] M. Ying,[130] J. Yokoyama,[28,27] T. Yokozawa,[189] J. Yoo,[179] T. Yoshioka,[199] Hang Yu,[136] Haocun Yu,[75] H. Yuzurihara,[187] A. Zadrożny,[218] M. Zanolin,[36] S. Zeidler,[288] T. Zelenova,[47] J.-P. Zendri,[82] M. Zevin,[164] M. Zhan,[177] H. Zhang,[230] J. Zhang,[94] L. Zhang,[1] R. Zhang,[77] T. Zhang,[14] Y. Zhang,[184] C. Zhao,[94] G. Zhao,[144] Y. Zhao,[187,20] Yue Zhao,[158] R. Zhou,[190] Z. Zhou,[15] X. J. Zhu,[5] Z.-H. Zhu,[120,228] M. E. Zucker,[1,75] and J. Zweizig[1]

(LIGO Scientific Collaboration, Virgo Collaboration, and KAGRA Collaboration)

[1]*LIGO Laboratory, California Institute of Technology, Pasadena, California 91125, USA*
[2]*Graduate School of Science, Tokyo Institute of Technology, Meguro-ku, Tokyo 152-8551, Japan*
[3]*Dipartimento di Farmacia, Università di Salerno, I-84084 Fisciano, Salerno, Italy*
[4]*INFN, Sezione di Napoli, Complesso Universitario di Monte S. Angelo, I-80126 Napoli, Italy*
[5]*OzGrav, School of Physics and Astronomy, Monash University, Clayton 3800, Victoria, Australia*
[6]*University of Wisconsin-Milwaukee, Milwaukee, Wisconsin 53201, USA*
[7]*Louisiana State University, Baton Rouge, Louisiana 70803, USA*
[8]*OzGrav, Australian National University, Canberra, Australian Capital Territory 0200, Australia*
[9]*Max Planck Institute for Gravitational Physics (Albert Einstein Institute), D-30167 Hannover, Germany*
[10]*Leibniz Universität Hannover, D-30167 Hannover, Germany*
[11]*Inter-University Centre for Astronomy and Astrophysics, Pune 411007, India*
[12]*University of Cambridge, Cambridge CB2 1TN, United Kingdom*

[13]*Theoretisch-Physikalisches Institut, Friedrich-Schiller-Universität Jena, D-07743 Jena, Germany*
[14]*University of Birmingham, Birmingham B15 2TT, United Kingdom*
[15]*Northwestern University, Evanston, Illinois 60208, USA*
[16]*Instituto Nacional de Pesquisas Espaciais, 12227-010 Sáo José dos Campos, São Paulo, Brazil*
[17]*Cardiff University, Cardiff CF24 3AA, United Kingdom*
[18]*INFN, Sezione di Pisa, I-56127 Pisa, Italy*
[19]*International Centre for Theoretical Sciences, Tata Institute of Fundamental Research, Bengaluru 560089, India*
[20]*Gravitational Wave Science Project, National Astronomical Observatory of Japan (NAOJ), Mitaka City, Tokyo 181-8588, Japan*
[21]*Advanced Technology Center, National Astronomical Observatory of Japan (NAOJ), Mitaka City, Tokyo 181-8588, Japan*
[22]*Dipartimento di Fisica, Università degli Studi di Torino, I-10125 Torino, Italy*
[23]*INFN Sezione di Torino, I-10125 Torino, Italy*
[24]*SUPA, University of Glasgow, Glasgow G12 8QQ, United Kingdom*
[25]*Università di Napoli "Federico II", Complesso Universitario di Monte S. Angelo, I-80126 Napoli, Italy*
[26]*Université de Lyon, Université Claude Bernard Lyon 1, CNRS, Institut Lumière Matière, F-69622 Villeurbanne, France*
[27]*Department of Physics, The University of Tokyo, Bunkyo-ku, Tokyo 113-0033, Japan*
[28]*Research Center for the Early Universe (RESCEU), The University of Tokyo, Bunkyo-ku, Tokyo 113-0033, Japan*
[29]*Institut de Ciències del Cosmos (ICCUB), Universitat de Barcelona, C/ Martí i Franquès 1, Barcelona, 08028, Spain*
[30]*University Savoie Mont Blanc, CNRS, Laboratoire d'Annecy de Physique des Particules—IN2P3, F-74000 Annecy, France*
[31]*Institut de Física d'Altes Energies (IFAE), Barcelona Institute of Science and Technology, and ICREA, E-08193 Barcelona, Spain*
[32]*Gran Sasso Science Institute (GSSI), I-67100 L'Aquila, Italy*
[33]*SUPA, University of Strathclyde, Glasgow G1 1XQ, United Kingdom*
[34]*Dipartimento di Scienze Matematiche, Informatiche e Fisiche, Università di Udine, I-33100 Udine, Italy*
[35]*INFN, Sezione di Trieste, I-34127 Trieste, Italy*
[36]*Embry-Riddle Aeronautical University, Prescott, Arizona 86301, USA*
[37]*Artemis, Université Côte d'Azur, Observatoire de la Côte d'Azur, CNRS, F-06304 Nice, France*
[38]*GRAPPA, Anton Pannekoek Institute for Astronomy and Institute for High-Energy Physics, University of Amsterdam, Science Park 904, 1098 XH Amsterdam, Netherlands*
[39]*Department of Physics, National and Kapodistrian University of Athens, School of Science Building, 2nd floor, Panepistimiopolis, 15771 Ilissia, Greece*
[40]*INFN, Sezione di Perugia, I-06123 Perugia, Italy*
[41]*Università di Camerino, Dipartimento di Fisica, I-62032 Camerino, Italy*
[42]*American University, Washington, D.C. 20016, USA*
[43]*Earthquake Research Institute, The University of Tokyo, Bunkyo-ku, Tokyo 113-0032, Japan*
[44]*California State University Fullerton, Fullerton, California 92831, USA*
[45]*Université de Paris, CNRS, Astroparticule et Cosmologie, F-75006 Paris, France*
[46]*Université Paris-Saclay, CNRS/IN2P3, IJCLab, 91405 Orsay, France*
[47]*European Gravitational Observatory (EGO), I-56021 Cascina, Pisa, Italy*
[48]*Georgia Institute of Technology, Atlanta, Georgia 30332, USA*
[49]*Chennai Mathematical Institute, Chennai 603103, India*
[50]*Department of Mathematics and Physics, Hirosaki University, 036-8560 Aomori, Hirosaki, Bunkyocho, 1, Japan*
[51]*Columbia University, New York, New York 10027, USA*
[52]*University of Portsmouth, Portsmouth PO1 3FX, United Kingdom*
[53]*Kamioka Branch, National Astronomical Observatory of Japan (NAOJ), Kamioka-cho, Hida City, Gifu 506-1205, Japan*
[54]*The Graduate University for Advanced Studies (SOKENDAI), Mitaka City, Tokyo 181-8588, Japan*
[55]*Università degli Studi di Urbino "Carlo Bo", I-61029 Urbino, Italy*
[56]*INFN, Sezione di Firenze, I-50019 Sesto Fiorentino, Firenze, Italy*
[57]*LIGO Livingston Observatory, Livingston, Louisiana 70754, USA*
[58]*INFN, Sezione di Roma, I-00185 Roma, Italy*
[59]*Université catholique de Louvain, B-1348 Louvain-la-Neuve, Belgium*
[60]*Nikhef, Science Park 105, 1098 XG Amsterdam, Netherlands*

[61]*King's College London, University of London, London WC2R 2LS, United Kingdom*
[62]*Korea Institute of Science and Technology Information, Daejeon 34141, Republic of Korea*
[63]*National Institute for Mathematical Sciences, Daejeon 34047, Republic of Korea*
[64]*Christopher Newport University, Newport News, Virginia 23606, USA*
[65]*School of High Energy Accelerator Science, The Graduate University for Advanced Studies (SOKENDAI), Tsukuba City, Ibaraki 305-0801, Japan*
[66]*Institute for Gravitational and Subatomic Physics (GRASP), Utrecht University, Princetonplein 1, 3584 CC Utrecht, Netherlands*
[67]*University of Oregon, Eugene, Oregon 97403, USA*
[68]*Syracuse University, Syracuse, New York 13244, USA*
[69]*Université de Liège, B-4000 Liège, Belgium*
[70]*Università degli Studi di Milano-Bicocca, I-20126 Milano, Italy*
[71]*INFN, Sezione di Milano-Bicocca, I-20126 Milano, Italy*
[72]*INAF, Osservatorio Astronomico di Brera sede di Merate, I-23807 Merate, Lecco, Italy*
[73]*LIGO Hanford Observatory, Richland, Washington 99352, USA*
[74]*Dipartimento di Medicina, Chirurgia e Odontoiatria "Scuola Medica Salernitana," Università di Salerno, I-84081 Baronissi, Salerno, Italy*
[75]*LIGO Laboratory, Massachusetts Institute of Technology, Cambridge, Massachusetts 02139, USA*
[76]*Wigner RCP, RMKI, H-1121 Budapest, Konkoly Thege Miklós út 29-33, Hungary*
[77]*University of Florida, Gainesville, Florida 32611, USA*
[78]*Stanford University, Stanford, California 94305, USA*
[79]*Università di Pisa, I-56127 Pisa, Italy*
[80]*Università di Perugia, I-06123 Perugia, Italy*
[81]*Università di Padova, Dipartimento di Fisica e Astronomia, I-35131 Padova, Italy*
[82]*INFN, Sezione di Padova, I-35131 Padova, Italy*
[83]*Bard College, Annandale-On-Hudson, New York 12504, USA*
[84]*Montana State University, Bozeman, Montana 59717, USA*
[85]*Institute for Plasma Research, Bhat, Gandhinagar 382428, India*
[86]*Universiteit Gent, B-9000 Gent, Belgium*
[87]*Nicolaus Copernicus Astronomical Center, Polish Academy of Sciences, 00-716, Warsaw, Poland*
[88]*Dipartimento di Ingegneria, Università del Sannio, I-82100 Benevento, Italy*
[89]*OzGrav, University of Adelaide, Adelaide, South Australia 5005, Australia*
[90]*The University of Texas Rio Grande Valley, Brownsville, Texas 78520, USA*
[91]*California State University, Los Angeles, Los Angeles, California 90032, USA*
[92]*Departamento de Matemáticas, Universitat Autònoma de Barcelona, Edificio C Facultad de Ciencias 08193 Bellaterra (Barcelona), Spain*
[93]*INFN, Sezione di Genova, I-16146 Genova, Italy*
[94]*OzGrav, University of Western Australia, Crawley, Western Australia 6009, Australia*
[95]*RRCAT, Indore, Madhya Pradesh 452013, India*
[96]*Missouri University of Science and Technology, Rolla, Missouri 65409, USA*
[97]*Vrije Universiteit Amsterdam, 1081 HV Amsterdam, Netherlands*
[98]*Lomonosov Moscow State University, Moscow 119991, Russia*
[99]*Università di Trento, Dipartimento di Fisica, I-38123 Povo, Trento, Italy*
[100]*INFN, Trento Institute for Fundamental Physics and Applications, I-38123 Povo, Trento, Italy*
[101]*SUPA, University of the West of Scotland, Paisley PA1 2BE, United Kingdom*
[102]*Bar-Ilan University, Ramat Gan, 5290002, Israel*
[103]*Dipartimento di Fisica "E.R. Caianiello," Università di Salerno, I-84084 Fisciano, Salerno, Italy*
[104]*INFN, Sezione di Napoli, Gruppo Collegato di Salerno, Complesso Universitario di Monte S. Angelo, I-80126 Napoli, Italy*
[105]*Università di Roma "La Sapienza", I-00185 Roma, Italy*
[106]*Univ Rennes, CNRS, Institut FOTON—UMR6082, F-3500 Rennes, France*
[107]*Indian Institute of Technology Bombay, Powai, Mumbai 400 076, India*
[108]*INFN, Laboratori Nazionali del Gran Sasso, I-67100 Assergi, Italy*
[109]*Laboratoire Kastler Brossel, Sorbonne Université, CNRS, ENS-Université PSL, Collège de France, F-75005 Paris, France*
[110]*Astronomical Observatory Warsaw University, 00-478 Warsaw, Poland*
[111]*University of Maryland, College Park, Maryland 20742, USA*
[112]*Max Planck Institute for Gravitational Physics (Albert Einstein Institute), D-14476 Potsdam, Germany*
[113]*L2IT, Laboratoire des 2 Infinis—Toulouse, Université de Toulouse, CNRS/IN2P3, UPS, F-31062 Toulouse Cedex 9, France*

[114]Villanova University, Villanova, Pennsylvania 19085, USA
[115]IGFAE, Universidade de Santiago de Compostela, 15782 Santiago de Compostela, Spain
[116]Stony Brook University, Stony Brook, New York 11794, USA
[117]Center for Computational Astrophysics, Flatiron Institute, New York, New York 10010, USA
[118]NASA Goddard Space Flight Center, Greenbelt, Maryland 20771, USA
[119]Dipartimento di Fisica, Università degli Studi di Genova, I-16146 Genova, Italy
[120]Department of Astronomy, Beijing Normal University, Beijing 100875, China
[121]OzGrav, University of Melbourne, Parkville, Victoria 3010, Australia
[122]Università degli Studi di Sassari, I-07100 Sassari, Italy
[123]INFN, Laboratori Nazionali del Sud, I-95125 Catania, Italy
[124]Università di Roma Tor Vergata, I-00133 Roma, Italy
[125]INFN, Sezione di Roma Tor Vergata, I-00133 Roma, Italy
[126]University of Sannio at Benevento, I-82100 Benevento, Italy and INFN, Sezione di Napoli, I-80100 Napoli, Italy
[127]Departamento de Astronomía y Astrofísica, Universitat de València, E-46100 Burjassot, València, Spain
[128]Universität Hamburg, D-22761 Hamburg, Germany
[129]Rochester Institute of Technology, Rochester, New York 14623, USA
[130]National Tsing Hua University, Hsinchu City, 30013 Taiwan, Republic of China
[131]The Chinese University of Hong Kong, Shatin, NT, Hong Kong
[132]Department of Applied Physics, Fukuoka University, Jonan, Fukuoka City, Fukuoka 814-0180, Japan
[133]OzGrav, Charles Sturt University, Wagga Wagga, New South Wales 2678, Australia
[134]Department of Physics, Tamkang University, Danshui District, New Taipei City 25137, Taiwan
[135]Department of Physics, Center for High Energy and High Field Physics, National Central University, Zhongli District, Taoyuan City 32001, Taiwan
[136]CaRT, California Institute of Technology, Pasadena, California 91125, USA
[137]Dipartimento di Ingegneria Industriale (DIIN), Università di Salerno, I-84084 Fisciano, Salerno, Italy
[138]Institute of Physics, Academia Sinica, Nankang, Taipei 11529, Taiwan
[139]Université Lyon, Université Claude Bernard Lyon 1, CNRS, IP2I Lyon/IN2P3, UMR 5822, F-69622 Villeurbanne, France
[140]INAF, Osservatorio Astronomico di Padova, I-35122 Padova, Italy
[141]OzGrav, Swinburne University of Technology, Hawthorn, Victoria 3122, Australia
[142]Université libre de Bruxelles, Avenue Franklin Roosevelt 50–1050 Bruxelles, Belgium
[143]IAC3–IEEC, Universitat de les Illes Balears, E-07122 Palma de Mallorca, Spain
[144]Université Libre de Bruxelles, Brussels 1050, Belgium
[145]Departamento de Matemáticas, Universitat de València, E-46100 Burjassot, València, Spain
[146]Texas Tech University, Lubbock, Texas 79409, USA
[147]University of Minnesota, Minneapolis, Minnesota 55455, USA
[148]The Pennsylvania State University, University Park, Pennsylvania 16802, USA
[149]University of Rhode Island, Kingston, Rhode Island 02881, USA
[150]Bellevue College, Bellevue, Washington 98007, USA
[151]Scuola Normale Superiore, Piazza dei Cavalieri, 7–56126 Pisa, Italy
[152]Eötvös University, Budapest 1117, Hungary
[153]Maastricht University, P.O. Box 616, 6200 MD Maastricht, Netherlands
[154]The University of Sheffield, Sheffield S10 2TN, United Kingdom
[155]Université Lyon, Université Claude Bernard Lyon 1, CNRS, Laboratoire des Matériaux Avancés (LMA), IP2I Lyon/IN2P3, UMR 5822, F-69622 Villeurbanne, France
[156]Dipartimento di Scienze Matematiche, Fisiche e Informatiche, Università di Parma, I-43124 Parma, Italy
[157]INFN, Sezione di Milano Bicocca, Gruppo Collegato di Parma, I-43124 Parma, Italy
[158]The University of Utah, Salt Lake City, Utah 84112, USA
[159]Carleton College, Northfield, Minnesota 55057, USA
[160]University of Zurich, Winterthurerstrasse 190, 8057 Zurich, Switzerland
[161]Perimeter Institute, Waterloo, Ontario N2L 2Y5, Canada
[162]Université de Strasbourg, CNRS, IPHC UMR 7178, F-67000 Strasbourg, France
[163]West Virginia University, Morgantown, West Virginia 26506, USA
[164]University of Chicago, Chicago, Illinois 60637, USA
[165]Montclair State University, Montclair, New Jersey 07043, USA
[166]Colorado State University, Fort Collins, Colorado 80523, USA
[167]Institute for Nuclear Research, Bem t'er 18/c, H-4026 Debrecen, Hungary

[168]*University of Texas, Austin, Texas 78712, USA*
[169]*CNR-SPIN, c/o Università di Salerno, I-84084 Fisciano, Salerno, Italy*
[170]*Scuola di Ingegneria, Università della Basilicata, I-85100 Potenza, Italy*
[171]*Observatori Astronòmic, Universitat de València, E-46980 Paterna, València, Spain*
[172]*Centro de Física das Universidades do Minho e do Porto, Universidade do Minho, Campus de Gualtar, PT-4710–057 Braga, Portugal*
[173]*Department of Astronomy, The University of Tokyo, Mitaka City, Tokyo 181-8588, Japan*
[174]*Faculty of Engineering, Niigata University, Nishi-ku, Niigata City, Niigata 950-2181, Japan*
[175]*Department of Physics, Graduate School of Science, Osaka City University, Sumiyoshi-ku, Osaka City, Osaka 558-8585, Japan*
[176]*Vanderbilt University, Nashville, Tennessee 37235, USA*
[177]*State Key Laboratory of Magnetic Resonance and Atomic and Molecular Physics, Innovation Academy for Precision Measurement Science and Technology (APM), Chinese Academy of Sciences, Xiao Hong Shan, Wuhan 430071, China*
[178]*University of Szeged, Dóm tér 9, Szeged 6720, Hungary*
[179]*Cornell University, Ithaca, New York 14850, USA*
[180]*University of British Columbia, Vancouver, British Columbia V6T 1Z4, Canada*
[181]*INAF, Osservatorio Astronomico di Capodimonte, I-80131 Napoli, Italy*
[182]*The University of Mississippi, University, Mississippi 38677, USA*
[183]*University of Michigan, Ann Arbor, Michigan 48109, USA*
[184]*Texas A&M University, College Station, Texas 77843, USA*
[185]*Ulsan National Institute of Science and Technology, Ulsan 44919, Republic of Korea*
[186]*Shanghai Astronomical Observatory, Chinese Academy of Sciences, Shanghai 200030, China*
[187]*Institute for Cosmic Ray Research (ICRR), KAGRA Observatory, The University of Tokyo, Kashiwa City, Chiba 277-8582, Japan*
[188]*Faculty of Science, University of Toyama, Toyama City, Toyama 930-8555, Japan*
[189]*Institute for Cosmic Ray Research (ICRR), KAGRA Observatory, The University of Tokyo, Kamioka-cho, Hida City, Gifu 506-1205, Japan*
[190]*University of California, Berkeley, California 94720, USA*
[191]*Maastricht University, 6200 MD, Maastricht, Netherlands*
[192]*Lancaster University, Lancaster LA1 4YW, United Kingdom*
[193]*College of Industrial Technology, Nihon University, Narashino City, Chiba 275-8575, Japan*
[194]*Rutherford Appleton Laboratory, Didcot OX11 0DE, United Kingdom*
[195]*Department of Astronomy and Space Science, Chungnam National University, Yuseong-gu, Daejeon 34134, Republic of Korea*
[196]*Department of Physical Sciences, Aoyama Gakuin University, Sagamihara City, Kanagawa 252-5258, Japan*
[197]*Kavli Institute for Astronomy and Astrophysics, Peking University, Haidian District, Beijing 100871, China*
[198]*Department of Physics, Aristotle University of Thessaloniki, University Campus, 54124 Thessaloniki, Greece*
[199]*Graduate School of Science and Engineering, University of Toyama, Toyama City, Toyama 930-8555, Japan*
[200]*Nambu Yoichiro Institute of Theoretical and Experimental Physics (NITEP), Osaka City University, Sumiyoshi-ku, Osaka City, Osaka 558-8585, Japan*
[201]*Directorate of Construction, Services and Estate Management, Mumbai 400094, India*
[202]*Universiteit Antwerpen, Prinsstraat 13, 2000 Antwerpen, Belgium*
[203]*University of Białystok, 15-424 Białystok, Poland*
[204]*Ewha Womans University, Seoul 03760, Republic of Korea*
[205]*National Astronomical Observatories, Chinese Academic of Sciences, Chaoyang District, Beijing, China*
[206]*School of Astronomy and Space Science, University of Chinese Academy of Sciences, Chaoyang District, Beijing, China*
[207]*University of Southampton, Southampton SO17 1BJ, United Kingdom*
[208]*Institute for Cosmic Ray Research (ICRR), The University of Tokyo, Kashiwa City, Chiba 277-8582, Japan*
[209]*Institute for High-Energy Physics, University of Amsterdam, Science Park 904, 1098 XH Amsterdam, Netherlands*
[210]*Chung-Ang University, Seoul 06974, Republic of Korea*
[211]*University of Washington Bothell, Bothell, Washington 98011, USA*

[212]Institute of Applied Physics, Nizhny Novgorod, 603950, Russia
[213]Inje University Gimhae, South Gyeongsang 50834, Republic of Korea
[214]Department of Physics, Myongji University, Yongin 17058, Republic of Korea
[215]Institute of Particle and Nuclear Studies (IPNS), High Energy Accelerator Research Organization (KEK), Tsukuba City, Ibaraki 305-0801, Japan
[216]School of Physics and Astronomy, Cardiff University, Cardiff, CF24 3AA, UK
[217]Institute of Mathematics, Polish Academy of Sciences, 00656 Warsaw, Poland
[218]National Center for Nuclear Research, 05-400 Świerk-Otwock, Poland
[219]Instituto de Fisica Teorica, 28049 Madrid, Spain
[220]Department of Physics, Nagoya University, Chikusa-ku, Nagoya, Aichi 464-8602, Japan
[221]Université de Montréal/Polytechnique, Montreal, Quebec H3T 1J4, Canada
[222]Laboratoire Lagrange, Université Côte d'Azur, Observatoire Côte d'Azur, CNRS, F-06304 Nice, France
[223]Seoul National University, Seoul 08826, Republic of Korea
[224]Sungkyunkwan University, Seoul 03063, Republic of Korea
[225]NAVIER, École des Ponts, Univ Gustave Eiffel, CNRS, Marne-la-Vallée, France
[226]Università di Firenze, Sesto Fiorentino I-50019, Italy
[227]Department of Physics, National Cheng Kung University, Tainan City 701, Taiwan
[228]School of Physics and Technology, Wuhan University, Wuhan, Hubei 430072, China
[229]National Center for High-performance computing, National Applied Research Laboratories, Hsinchu Science Park, Hsinchu City 30076, Taiwan
[230]Department of Physics, National Taiwan Normal University, Sec. 4, Taipei 116, Taiwan
[231]NASA Marshall Space Flight Center, Huntsville, Alabama 35811, USA
[232]INFN, Sezione di Roma Tre, I-00146 Roma, Italy
[233]ESPCI, CNRS, F-75005 Paris, France
[234]Kenyon College, Gambier, Ohio 43022, USA
[235]School of Physics Science and Engineering, Tongji University, Shanghai 200092, China
[236]Dipartimento di Fisica, Università di Trieste, I-34127 Trieste, Italy
[237]Institute for Photon Science and Technology, The University of Tokyo, Bunkyo-ku, Tokyo 113-8656, Japan
[238]Indian Institute of Technology Madras, Chennai 600036, India
[239]Saha Institute of Nuclear Physics, Bidhannagar, West Bengal 700064, India
[240]Institute of Space and Astronautical Science (JAXA), Chuo-ku, Sagamihara City, Kanagawa 252-0222, Japan
[241]Institut des Hautes Etudes Scientifiques, F-91440 Bures-sur-Yvette, France
[242]Faculty of Law, Ryukoku University, Fushimi-ku, Kyoto City, Kyoto 612-8577, Japan
[243]Indian Institute of Science Education and Research, Kolkata, Mohanpur, West Bengal 741252, India
[244]Department of Physics, University of Notre Dame, Notre Dame, Indiana 46556, USA
[245]Graduate School of Science and Technology, Niigata University, Nishi-ku, Niigata City, Niigata 950-2181, Japan
[246]Consiglio Nazionale delle Ricerche—Istituto dei Sistemi Complessi, Piazzale Aldo Moro 5, I-00185 Roma, Italy
[247]Korea Astronomy and Space Science Institute (KASI), Yuseong-gu, Daejeon 34055, Republic of Korea
[248]Hobart and William Smith Colleges, Geneva, New York 14456, USA
[249]International Institute of Physics, Universidade Federal do Rio Grande do Norte, Natal RN 59078-970, Brazil
[250]Museo Storico della Fisica e Centro Studi e Ricerche "Enrico Fermi", I-00184 Roma, Italy
[251]Dipartimento di Matematica e Fisica, Università degli Studi Roma Tre, I-00146 Roma, Italy
[252]University of Arizona, Tucson, Arizona 85721, USA
[253]Università di Trento, Dipartimento di Matematica, I-38123 Povo, Trento, Italy
[254]University of California, Riverside, Riverside, California 92521, USA
[255]University of Washington, Seattle, Washington 98195, USA
[256]Indian Institute of Technology, Palaj, Gandhinagar, Gujarat 382355, India
[257]Department of Electronic Control Engineering, National Institute of Technology, Nagaoka College, Nagaoka City, Niigata 940-8532, Japan
[258]Departamento de Matemática da Universidade de Aveiro and Centre for Research and Development in Mathematics and Applications, Campus de Santiago, 3810-183 Aveiro, Portugal
[259]Marquette University, Milwaukee, Wisconsin 53233, USA
[260]Faculty of Science, Toho University, Funabashi City, Chiba 274-8510, Japan
[261]Graduate School of Science and Technology, Gunma University, Maebashi, Gunma 371-8510, Japan

[262]*Institute for Quantum Studies, Chapman University, Orange, California 92866, USA*
[263]*Accelerator Laboratory, High Energy Accelerator Research Organization (KEK), Tsukuba City, Ibaraki 305-0801, Japan*
[264]*Faculty of Information Science and Technology, Osaka Institute of Technology, Hirakata City, Osaka 573-0196, Japan*
[265]*INAF, Osservatorio Astrofisico di Arcetri, Largo E. Fermi 5, I-50125 Firenze, Italy*
[266]*Indian Institute of Technology Hyderabad, Sangareddy, Khandi, Telangana 502285, India*
[267]*Indian Institute of Science Education and Research, Pune, Maharashtra 411008, India*
[268]*Istituto di Astrofisica e Planetologia Spaziali di Roma, Via del Fosso del Cavaliere, 100, 00133 Roma RM, Italy*
[269]*Department of Space and Astronautical Science, The Graduate University for Advanced Studies (SOKENDAI), Sagamihara City, Kanagawa 252-5210, Japan*
[270]*Andrews University, Berrien Springs, Michigan 49104, USA*
[271]*Research Center for Space Science, Advanced Research Laboratories, Tokyo City University, Setagaya, Tokyo 158-0082, Japan*
[272]*Institute for Cosmic Ray Research (ICRR), Research Center for Cosmic Neutrinos (RCCN), The University of Tokyo, Kashiwa City, Chiba 277-8582, Japan*
[273]*Department of Physics, Kyoto University, Sakyou-ku, Kyoto City, Kyoto 606-8502, Japan*
[274]*Yukawa Institute for Theoretical Physics (YITP), Kyoto University, Sakyou-ku, Kyoto City, Kyoto 606-8502, Japan*
[275]*Dipartimento di Scienze Aziendali—Management and Innovation Systems (DISA-MIS), Università di Salerno, I-84084 Fisciano, Salerno, Italy*
[276]*Van Swinderen Institute for Particle Physics and Gravity, University of Groningen, Nijenborgh 4, 9747 AG Groningen, Netherlands*
[277]*Faculty of Science, Department of Physics, The Chinese University of Hong Kong, Shatin, N.T., Hong Kong*
[278]*Vrije Universiteit Brussel, Pleinlaan 2, 1050 Brussel, Belgium*
[279]*Applied Research Laboratory, High Energy Accelerator Research Organization (KEK), Tsukuba City, Ibaraki 305-0801, Japan*
[280]*Department of Communications Engineering, National Defense Academy of Japan, Yokosuka City, Kanagawa 239-8686, Japan*
[281]*Department of Physics, University of Florida, Gainesville, Florida 32611, USA*
[282]*Department of Information and Management Systems Engineering, Nagaoka University of Technology, Nagaoka City, Niigata 940-2188, Japan*
[283]*Tata Institute of Fundamental Research, Mumbai 400005, India*
[284]*Eindhoven University of Technology, Postbus 513, 5600 MB Eindhoven, Netherlands*
[285]*Department of Physics and Astronomy, Sejong University, Gwangjin-gu, Seoul 143-747, Republic of Korea*
[286]*Concordia University Wisconsin, Mequon, Wisconsin 53097, USA*
[287]*Department of Electrophysics, National Yang Ming Chiao Tung University, Hsinchu, Taiwan*
[288]*Department of Physics, Rikkyo University, Toshima-ku, Tokyo 171-8501, Japan*

[†]Deceased.